SOUND SPEED DISPERSION, ATTENUATION AND INFERRED MICROBUBBLES IN THE UPPER OCEAN

Thomas Bartlett Huffman

NAVAL POSTGRADUATE SCHOOL
Monterey, California

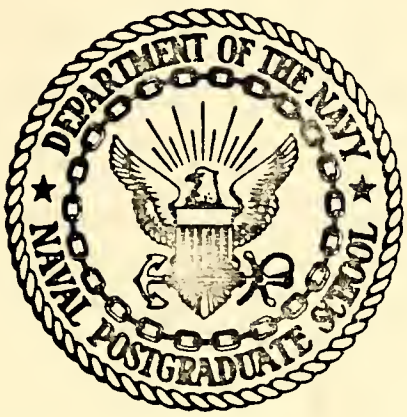

THESIS

SOUND SPEED DISPERSION, ATTENUATION AND INFERRED MICROBUBBLES IN THE UPPER OCEAN

by

Thomas Bartlett Huffman
and
Dennis Leeth Zveare

December 1974

Thesis Advisor: H. Medwin

Approved for public release; distribution unlimited.

UNCLASSIFIED

SECURITY CLASSIFICATION OF THIS PAGE (When Data Entered)

REPORT DOCUMENTATION PAGE		READ INSTRUCTIONS BEFORE COMPLETING FORM
1. REPORT NUMBER	2. GOVT ACCESSION NO.	3. RECIPIENT'S CATALOG NUMBER
4. TITLE (and Subtitle) Sound Speed Dispersion, Attenuation and Inferred Microbubbles in the Upper Ocean		5. TYPE OF REPORT & PERIOD COVERED Master's Thesis; December 1974 6. PERFORMING ORG. REPORT NUMBER
7. AUTHOR(s) Thomas Bartlett Huffman Dennis Leeth Zveare		8. CONTRACT OR GRANT NUMBER(s)
9. PERFORMING ORGANIZATION NAME AND ADDRESS Naval Postgraduate School Monterey, California 93940		10. PROGRAM ELEMENT, PROJECT, TASK AREA & WORK UNIT NUMBERS
11. CONTROLLING OFFICE NAME AND ADDRESS Naval Postgraduate School Monterey, California 93940		12. REPORT DATE December 1974 13. NUMBER OF PAGES 123
14. MONITORING AGENCY NAME & ADDRESS(if different from Controlling Office) Naval Postgraduate School Monterey, California 93940		15. SECURITY CLASS. (of this report) Unclassified 15a. DECLASSIFICATION/DOWNGRADING SCHEDULE

16. DISTRIBUTION STATEMENT (of this Report)

Approved for public release; distribution unlimited.

17. DISTRIBUTION STATEMENT (of the abstract entered in Block 20, if different from Report)

18. SUPPLEMENTARY NOTES

19. KEY WORDS (Continue on reverse side if necessary and identify by block number)

Underwater Sound
Speed of Sound
Sound Amplitude
Bubbles
Upper Ocean
Dispersion
Attenuation

20. ABSTRACT (Continue on reverse side if necessary and identify by block number)

A portable underwater source-receiver system, supporting equipment, and digital computer software have been developed to determine near-surface sound speed and attenuation at harmonic frequencies from 5 to 95 kHz simultaneously, and in-situ from a ship. These data have yielded values of bubble densities as a function of bubble radius from 40 to 1000 microns, depth to 15.2 meters, time of day, varying oceanographic

DD FORM 1 JAN 73 1473 (Page 1)

EDITION OF 1 NOV 65 IS OBSOLETE
S/N 0102-014-6601

UNCLASSIFIED

SECURITY CLASSIFICATION OF THIS PAGE (When Data Entered)

conditions and environmental parameters for two days in November in Monterey Bay.

Sound Speed Dispersion, Attenuation and Inferred Microbubbles in the Upper Ocean

by

Thomas Bartlett Huffman
Lieutenant, United States Navy
B.S., United States Naval Academy, 1966

Dennis Leeth Zveare
Lieutenant, United States Navy
B.S., United States Naval Academy, 1966

Submitted in partial fulfillment of the requirements for the degree of

MASTER OF SCIENCE IN ENGINEERING ACOUSTICS

from the

NAVAL POSTGRADUATE SCHOOL
December 1974

ABSTRACT

A portable underwater source-receiver system, supporting equipment, and digital computer software have been developed to determine near-surface sound speed and attenuation at harmonic frequencies from 5 to 95 kHz simultaneously, and in-situ from a ship. These data have yielded values of bubble densities as a function of bubble radius from 40 to 1000 microns, depth to 15.2 meters, time of day, varying oceanographic conditions and environmental parameters for two days in November in Monterey Bay.

TABLE OF CONTENTS

LIST OF DRAWINGS

ACKNOWLEDGEMENT

The authors would like to express sincere appreciation to their thesis advisor, Dr. Herman Medwin, for his guidance, direction, and, most of all, patience; to Mr. William "Bill" Smith, whose technical experience and expertise proved an invaluable asset in completion of this project; and to Mrs. Carol Hickey, whose rapport with the computer, "OPHELEA," enabled them to concentrate on the physics disciplines most germane to the research project. Special thanks are also due to Captain "Woody" Reynolds and his crew aboard the Research Vessel ACANIA, and to the many professors and technicians in all departments of the Postgraduate School who readily gave of their time and resources in support of this research.

This research work was supported by Office of Naval Research Code 480.

I. INTRODUCTION

A. BACKGROUND

When a sound wave propagates through the ocean, its intensity is weakened with increasing distance. There are two mechanisms which adequately explain this weakening: divergence and absorption. If we are given an infinite medium (i.e., no boundaries) that is also homogeneous and free from scatterers, this weakening is predictable. Spherical spreading changes the sound intensity in proportion to the inverse square of the range. Absorption weakens the sound as a function of frequency.

In the real ocean we can approach a test situation where boundary effects can be ignored. However, the nature of the sea makes it impossible to assume a homogeneous medium. It has been found through observations of sound waves in the ocean that both their amplitudes and phases fluctuate. This is to be expected since the ocean is, in fact, dynamic and is moved constantly by tide and current. As this transport of water past a fixed point occurs, the inhomogeneities also move, thereby altering the acoustic conditions along the sound path. In-situ measurements of the ocean microstructure are difficult to obtain by traditional methods.

Acoustic probing, since it does not alter the medium is an excellent research tool for learning about the structure

of the sea. This probing can be used to determine the presence of scatterers by observing their effect on both sound attenuation and sound speed as a function of frequency.

The presence of bubbles in the near-surface ocean causes additional attenuation and makes the phase speed dispersive. The near-surface frequency dependence of sound propagation is especially important with respect to naval sonars which often transmit their sound in a surface duct mode. This transmission could be subjected to unexpected errors if a bubble-free model of computing sound speed were used in an area containing a large population of resonant bubbles. If a close correlation can be found between bubble population density and weather conditions or environmental parameters, this would enable the Navy to publish sound speed and attenuation corrections to sonar performance tables which could be applied aboard the individual ship according to the existing conditions.

B. OBJECTIVE

The objective of this research was to take in-situ acoustic measurements over a fixed range of approximately one meter in the upper fifteen meters of the ocean in order to observe and record sound wave amplitudes and sound speeds as a function of frequency. These data were then reduced to compute bubble populations by size and depth and to compute a differential value of sound speed as a function of frequency in the upper reaches of the sea.

In order to make the observations, a constant amplitude sawtooth sound wave, rich in harmonic content, was transmitted horizontally through the sea past two acoustic receivers that were spatially fixed in the far field of the transducer. Signals received by these hydrophones were digitized and processed by a high-speed, high-resolution computer. Amplitudes recorded at various depths and locations, at various times, and under various oceanographic and meteorological conditions were spectrally analyzed, and were then related to bubble population of the medium. The computed phase angle of each harmonic permitted the calculation of the sound speed at that frequency. The computed propagation loss, compared to the bubble-free medium yielded the attenuation at that frequency.

C. BUBBLE ABSORPTION AND SCATTER THEORY

Bubbles have a drastic effect on amplitude attenuation if they are of such a size that they are at or near the resonance frequency of a transmitted component. If this situation exists, the bubbles resonate, thus absorbing and scattering that particular frequency component of the incident sound wave, and causing changes in the sound speed. It is this property of bubbles that was utilized in this research project to determine average bubble populations over the sound path.

Determination of bubble population by acoustic methods is shown to be theoretically practical by considering the

scattering cross section, σ_s, and the absorption cross section, σ_a, of a bubble. Computation shows that, at resonance, the scattering cross section of the most prominent bubbles is 180 to 900 times greater than the geometrical cross section and the absorption cross section is many times again larger than the scattering cross section [Medwin, 1970]. Because of this inordinately large effective bubble cross section at resonance in conjunction with an extremely narrow resonance peak, it is then quite easy to detect resonant bubbles even in the presence of non-resonant bubbles, fish, and particulate matter.

The size distribution of bubbles has been investigated by numerous research scientists. Most notably, efforts by Glotov [1962] and by Blanchard and Woodcock [1957] imply that the majority of bubbles encountered are below 200 microns radius with a population peak in the vicinity of 60 microns. Larger bubbles tend to rise rapidly to the surface and disappear due to buoyancy. Smaller bubbles tend to shrink and disappear. This information indicates that a frequency range from 10 kHz to 100 kHz should effectively define the major bubble population. For this experiment, a range from 5 kHz to 100 kHz was chosen.

For present purposes, let us assume bubbles of a uniform size are present in a sound field. Further assume no bubbles of other sizes present, and that the number is small enough that interaction may be discounted. The attenuation due to the presence of these bubbles is then

the additive contribution caused by the extinction effect of each individual bubble. The extinction effect is the combined effect of absorption and scattering, that is, the extinction cross section, σ_e, is the sum of the scattering cross section, σ_s, and the absorption cross section, σ_a [Class Notes, Medwin, 1964].

$$\sigma_e = \sigma_s + \sigma_a \ , \tag{1}$$

where

$$\sigma_s = \frac{\text{Power scattered over all angles}}{\text{Incident Acoustic Intensity}}$$

$$= \frac{4\pi R_o^{\,2}}{((\omega_o/\omega)^2-1)^2+\delta^2} \tag{2}$$

$$\sigma_a = \frac{\text{Power absorbed by bubble}}{\text{Incident Acoustic Intensity}}$$

$$= \sigma_s(\delta/K_oR_o-1) \tag{3}$$

Therefore, after consolidation

$$\sigma_e = \left[\frac{4\pi R_o^{\,2}}{((\omega_o/\omega)^2-1)^2+\delta^2}\right]\left[\frac{\delta}{K_oR_o}\right], \tag{4}$$

where

R_0 = Resonant bubble radius,

ω = Angular frequency of incident sound,

ω_0 = Angular frequency of bubble pulsation at resonance,

δ = Total bubble damping constant,

$K_0 = \frac{2\pi}{\lambda_0}$ = Sound propagation constant at bubble resonance frequency.

If the intensity incident on the sound field is I_0, then the amount of power dissipated by an individual bubble is $I_0\sigma_e$. If we let N(R) equal the number of resonant bubbles present in a unit volume, then the change in intensity over a distance dx is

$$dI = -I_o\sigma_e N(R) e^{-\sigma_e N(R)x} dx \qquad (5)$$

after integration

$$I = I_o e^{-\sigma_e N(R)x} \qquad (6)$$

Expressing the change in intensity level, or attenuation, in decibels

$$\begin{aligned} \Delta I.L. &= 10 \operatorname{Log}_{10} \frac{I}{I_o} \\ &= -10\sigma_e N(R) x \operatorname{Log}_{10} e \\ &= 4.34\ \sigma_e N(R) x \end{aligned} \qquad (7)$$

Finally, expressing this attenuation relative to a unit distance,

$$\frac{\Delta I.L.}{x} = 4.34\ \sigma_e N(R) \qquad (8)$$

In-situ measurements of bubbles at sea, of course, involve bubbles of various sizes. It becomes necessary then, to determine the degree of response of near-resonant bubbles and the range of bubble sizes that will cause sound of a unique frequency to attenuate significantly over a known distance. From previous studies, it has been found that appreciable scattering and absorption will occur only for

frequencies relatively close to the resonance frequency. In fact, it has been found that if the frequency range, Δf, is equal to f_0 ± 0.045 times the resonant frequency, then the extinction cross section is only one half its resonance value [Class Notes, Medwin, 1964]. Thus, it follows that only bubbles of size quite close to resonant size will contribute to the extinction cross section.

To calculate this total extinction cross section, it will be necessary to integrate over a range of bubble radii. Theoretically, the integral will be over the entire range from zero to infinity. Practically, however, it has been shown that only a small range of sizes need be considered in close proximity to the resonant bubble size. Thus, our total extinction cross section, σ_E, reduces to

$$S_E = \int_{R_o}^{R_o+dR} \sigma_e n(R)dR = \int_{R}^{R+dR} \frac{4\pi R^2 (\delta/\delta_r) n(R)dR}{((\omega_o/\omega)^2-1)^2 + \delta^2} \quad (9)$$

where

$n(R)dR$ = Total number of bubbles per unit volume with radii between R_0 and R_0+dR,

δ_r = Resonant bubble damping constant,

= $K_0 R_0$ (1.36×10^{-2} for a clean air bubble in water at one atmosphere.

In view of the small range of radii considered for each resonance frequency, it is valid to assume the quantities $n(R)$, δ, and δ_r are constant over the range and, therefore,

treat them external to the integral. This yields

$$S_E = 4\pi(\delta/\delta_r)n(R)\int_{R_o}^{R_o+dR}\frac{R^2dR}{((\omega_o/\omega)^2+\delta^2} \qquad (10)$$

Next, it is necessary to express all variables in the integral in terms of a common variable.

Let $\mathcal{R} = \omega_0/\omega - 1 = R/R_0 - 1$.

Then $d\mathcal{R} = dR/R_0$.

Substituting

$$S_E = 4\pi(\delta/\delta_r)n(R)\int_{-\mathcal{R}}^{+\mathcal{R}}\frac{((\mathcal{R}+1)(R_o))^2R_o d\mathcal{R}}{((\mathcal{R}+1)^2-1)^2+\delta^2}$$

And, after consolidating terms

$$S_E = 4\pi R_o^3(\delta/\delta_r)n(R)\int_{-\mathcal{R}}^{+\mathcal{R}}\frac{(1+\mathcal{R})^2d\mathcal{R}}{((1+\mathcal{R})^2-1)^2+\delta^2} \qquad (11)$$

Now, simplifying by dropping higher order terms in $\mathcal{R}$, we arrive at

$$S_E \approx 4\pi R_o^3(\delta/\delta_r n(R)\int_{-\mathcal{R}}^{+\mathcal{R}}\frac{d\mathcal{R}}{4\mathcal{R}^2+\delta^2}$$

And, after integrating

$$S_E \approx 4\pi R_o^3(\delta/\delta_r)n(R)\left[1/\delta\ \mathrm{Tan}^{-1}\ 2\mathcal{R}/\delta\right]$$

$$= 4\pi R_o^3 n(R)/\delta_r\ \mathrm{Tan}^{-1}\ 2\mathcal{R}/\delta \qquad (12)$$

The maximum extinction cross section will occur when $\text{Tan}^{-1}\ 2\mathcal{R}/\delta = \pi/2$. If we choose reasonable, representative values for $\mathcal{R}$ and δ such as $\mathcal{R} = 0.1$ and $\delta = 0.1$, $\text{Tan}^{-1}\ 2\mathcal{R}/\delta = 0.71(\pi/2)$. Thus, bubbles within 10% of the resonant bubble size will cause 71% of the total extinction cross section.

For our purposes, and in order to predict the maximum extinction cross section with maximum attenuation, we will evaluate in the limit with $\text{Tan}^{-1}\ 2\mathcal{R}/\delta = \pi/2$. Thus, equation (12) reduces to

$$S_E = 2\pi^2 R_o^3 n(R)/\delta_r \qquad (13)$$

Returning to equation (8), the expression equating attenuation due to single size bubbles, we may now substitute our total extinction cross section, S_E, for $\sigma_e N(R)$, the extinction cross section for single radius bubbles. This substitution yields an expression for attenuation due to all bubble sizes.

$$a = 4.34\ S_E$$

$$= 4.34\ 2\pi^2 R_o^3 n(R)/\delta_r \qquad (14)$$

For a meaningful method of expressing the attenuation in terms of the volume of air in the bubbles, we can define $U(R)dR$ as the volume of air per unit volume of water for bubbles with radii between R_0 and R_0+dR. Assuming spherical bubbles, this quantity can be expressed

$$U(R)dR = 4/3\ \pi R_o^3 n(R)dR \qquad (15)$$

Cancelling and solving for $R_0^3\, n(R)$ yields

$$R_o^3 n(R) = 3/4\ \pi U(R) \qquad (16)$$

Substituting this expression into equation (14) and assuming a clean air bubble with $\delta_r = 1.36 \times 10^{-2}$

$$a = 1.50 \times 10^3\ U(R)\ \text{dB/meter} \qquad (17)$$

The next consideration of major importance is to calculate the size of a resonant bubble. The resonant relationship is [Eckart, 1945]

$$f_o = 1/2\pi\ R_o \sqrt{3\gamma P_o / \rho_o} \qquad (18)$$

where γ = Effective ratio of specific heats of bubble gas,

ρ_0 = Density of surrounding water,

P_0 = Ambient pressure at bubble depth,

τ = Measure of surface tension.

τ deviates only slightly from unity and then only for very small bubble radii, and thus can be discounted [Devin, 1959]. γ for clean air bubbles falls in the range $1.16 < \gamma \leq 1.40$ for bubbles larger than 20 microns. For prediction purposes, the value 1.40 will be used. This will cause an error no greater than 10% in resonant bubble radius. ρ_0 for sea water at 20° C and standard atmospheric pressure is 1026 Kg/M^3. Finally, ambient pressure at bubble depth may be calculated from the linear expression

$$P = 1.0\times10^{5}\left(1+\frac{\text{depth (meters)}}{10.337\ \text{meters}}\right)\frac{NT}{M^2} \qquad (19)$$

Thus, equation (18) reduces to

$$R_o = \frac{1.02\times10^{-2}}{f_o}\sqrt{P_o}\ \text{meters} \qquad (20)$$

Use of this equation yields TABLE 1, a compilation of resonant bubble radii as a function of frequency and depth, from the surface to 16 meters.

In order to demonstrate this theoretical approach, a sample computation will best demonstrate the application of the resonant bubble theory.

Given: 60 kHz sound source

Matched receivers at 5 meter depth

Unbounded salt water medium

One meter spatial path between receivers

Data yields excess attenuation from receiver one to receiver two of 1.00 dB relative to 15.2 meter bubble-free calibration depth

P_0 at 5 meter depth

$$P_o = 1.0\times10^{5}\left(1+\frac{5}{10.337}\right)\frac{NT}{M^2}$$

$$P_o = 1.5\times10^{5}\ \frac{NT}{M^2}$$

R_0 at 5 meter depth for 60 kHz signal

$$R = 1/2\pi\ f_o\left(3\gamma P_o/\rho_o\right)^{1/2}$$

$$= 1/2\pi\left[(60\times10^{3})\ 3(1.4)(1.5\times10^{5}/1026)\right]^{\frac{1}{2}}$$

$$\underline{R_{o} = 66 \text{ microns}}$$

$$a = 1.5\times10^{3}\ U(R)$$

$$U(R) = 1.0/1.5\times10^{3}$$

$$\underline{U(R) = 6.7\times10^{-4}\ m^{-1}}$$

Finally, solving equation (16) for the number of resonant bubbles in a 1 micron band

$$n(R)dR = 3/4\pi\ U(R)dR\ (1/R_{o}^{3})$$

$$n(R)dR = 3/4\ \ (6.7\times10^{-4})(1.0\times10^{-6})(1/66\times10^{-6})^{3}$$

$$\underline{n(R)dR = 556 \text{ resonant bubbles per cubic meter of radius } 66 \pm 0.5 \text{ microns}}$$

f (kHz)	1 meter	2 meter	3 meter	4 meter	5 meter	6 meter
	R_0 in microns					
5	675	703	731	759	783	809
10	338	351	366	380	392	405
15	225	234	244	253	261	270
20	169	176	183	190	196	202
25	135	141	146	152	157	162
30	113	117	122	127	131	135
35	96.5	100	104	108	112	116
40	84.4	87.8	91.4	94.9	97.9	101
45	75.1	78.1	81.3	84.4	87.0	89.9
50	67.5	70.3	73.1	75.9	78.3	80.9
55	61.4	63.9	66.5	69.0	71.2	73.6
60	56.3	58.5	61.0	63.3	65.3	67.5
65	52.0	54.0	56.3	58.4	60.3	62.3
70	48.2	50.2	52.2	54.2	56.0	57.8
75	45.0	46.8	48.8	50.6	52.2	54.0
80	42.2	43.9	45.7	47.4	49.0	50.6
85	39.7	41.3	43.0	44.7	46.1	47.6
90	37.5	39.0	40.6	42.2	43.5	45.0
95	35.6	37.0	38.5	40.0	41.2	42.6
100	33.8	35.1	36.6	38.0	39.2	40.5

RESONANT BUBBLE RADII AS A FUNCTION
OF FREQUENCY AND DEPTH

Assumptions: Clean Bubble Surface
$\gamma = 1.40$
No Surface Tension Effects
No Heat Conductivity Effects

TABLE 1

f (kHz)	7 meter	8 meter	9 meter	10 meter	11 meter	12 meter
	R_0 in microns					
5	835	857	881	904	924	947
10	417	428	440	452	462	473
15	278	286	249	301	308	316
20	209	214	220	226	231	237
25	167	171	176	181	185	189
30	139	143	147	151	154	158
35	119	122	126	129	132	135
40	104	107	110	113	116	118
45	92.7	95.2	97.9	100	103	105
50	83.5	85.7	88.1	90.4	92.4	94.7
55	75.9	77.9	80.1	82.2	84.0	86.1
60	69.6	71.4	73.4	75.3	77.0	78.9
65	64.2	65.9	67.8	69.5	71.1	72.8
70	59.6	61.2	62.9	64.6	66.0	67.6
75	55.6	57.1	58.7	60.3	61.6	63.1
80	52.2	53.6	55.0	56.5	57.8	59.2
85	49.1	50.4	51.8	53.2	54.4	55.7
90	46.4	47.6	48.9	50.2	51.4	52.6
95	43.9	45.1	46.4	47.6	48.7	49.8
100	41.7	42.8	44.0	45.2	46.2	47.3

f (kHz)	13 meter	14 meter	15 meter	15.24 meter	16 meter
	R_0 in microns				
5	968	987	1008	1012	1028
10	484	494	504	506	514
15	323	329	336	337	343
20	242	247	252	253	257
25	194	197	202	202	206
30	161	165	168	169	171
35	138	141	144	145	147
40	121	123	126	127	129
45	108	110	112	112	114
50	96.8	98.7	101	101	103
55	88.0	89.8	91.6	92.0	93.5
60	80.7	82.3	84.0	84.4	85.7
65	74.5	76.0	77.5	77.9	79.1
70	69.2	70.5	72.0	72.3	73.5
75	64.6	65.8	67.2	67.5	68.6
80	60.5	61.7	63.0	63.3	64.3
85	57.0	58.1	59.3	59.5	60.5
90	53.8	54.9	56.0	56.2	57.1
95	51.0	52.0	53.1	53.3	54.1
100	48.4	49.4	50.4	50.6	51.4

D. SOUND SPEED DISPERSION THEORY

The sound speed dispersion theory was described in Rautmann [1971] and Fitzgerald [1972], portions of which are included here for information.

The following equation relates bubble size to the speed of sound and indicates the speed dispersion for a bubble population of unique radius R_o

$$C = \left[\frac{1}{C_o} + \frac{3C_o}{2\omega^2} \frac{U(R_o)}{R_o^2} \frac{\left[\left(\frac{\omega_o}{\omega} \right)^2 - 1 \right]}{\left[\left(\frac{\omega_o}{\omega} \right) - 1 \right]^2 + \delta^2 \left(\frac{\omega_o}{\omega} \right)^2} \right]^{-1} \qquad (21)$$

C_o = nondispersive sound speed,

ω = sound frequency,

ω_o = resonant frequency of bubble of radius R_o,

$U(R_o)$ = fractional air-to-water volume of bubbles having radius R_o,

δ = damping constant of bubbles of radius R_o.

This relation predicts that in a region of bubbles with a unique radius and a resonance frequency ω_o, the sound speed will increase if an incident sound wave has a frequency greater than ω_o, and will decrease if the incident frequency is less than ω_o. Figure 1 shows typical sound speed changes in an area of unique bubble radii.

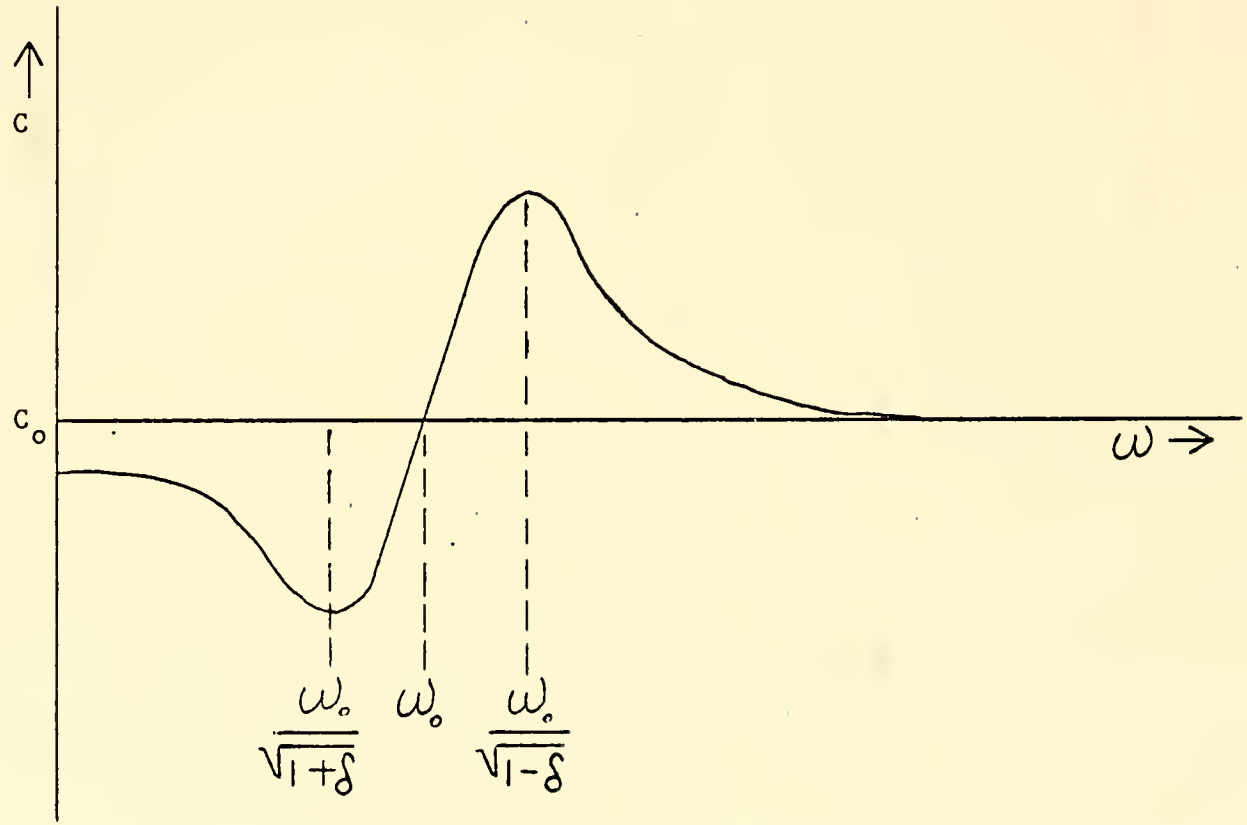

FIG. 1 EFFECT ON SOUND SPEED OF A UNIQUE RADIUS BUBBLE POPULATION

For frequencies far below the resonance frequencies of bubbles present in a mixture, $\omega << \omega_o$, equation 21 reduces to

$$C = C_o \left[1 - \frac{3U}{2(kR_o)^2} \right] \qquad (22)$$

A bubble population including several different bubble sizes would have the same equation predicting the speed of sound, except the fractional volumes and resonant frequency effects would have to be summed over all bubble radii present, causing a combination of several speed variation curves such as Figure 1, with the amplitudes of each proportional to the density of that particular sized bubble's population.

If a region of the ocean contained an unusually large population of bubbles near one resonant bubble size in comparison to the population of bubbles within ±20% of that size, a curve such as Figure 1 would be expected. Since bubbles have little effect on frequencies more than 20% removed from their resonance frequency, more than one such dispersion area could exist on the same curve centered on different frequencies. This would represent more than one unusually large population of bubbles centered around those resonant frequencies.

The computational method for determination of the speed of sound using the phase difference was the same as that used by Rautmann [1971] once the phase angle of each

component harmonic was given by either the Fast Fourier Transform or by using the phase meter. This method is repeated here.

Each harmonic frequency received by the first hydrophone can be written as:

$$y_A = a \sin(\omega t) \tag{23}$$

and the signal received by the second hydrophone is:

$$y_B = b \sin(\omega t - kx) \tag{24}$$

where

k = the wave number = $\frac{\omega}{C} = \frac{2\pi f}{C}$,

f = the frequency of the applied signal,

C = the wave phase speed,

x = the separation between the hydrophones.

Since we compare the two signals with respect to phase by using the digital phase meter or the FFT output we have to find values for which kx equals the total phase difference between the two signals due to an integral number of wave lengths and a fraction of the wave length. This is written as:

$$kx = (2\pi)n + \phi_r$$

$$kx = \frac{\omega}{C} x = (2\pi)n + \phi_r$$

$$C = \frac{\omega x}{(2\pi)n + \phi_r}$$

n = an integer

ϕ_r = fractional wave length in radians

(25)

The final result is:

$$C = \frac{fx}{n + \frac{\phi}{360}} \qquad \text{where } \phi \text{ is in degrees.} \qquad (26)$$

The integer n can be pre-estimated by calculating the number of wavelengths using the speed of sound given by the velocimeter.

II. THE EXPERIMENT

The theory of resonant bubble attenuation has been supported by previous theses. However, past research has been limited to analog time averaging of single frequencies with a sensor system suspended from a stationary platform. This research project has attempted to devise a system that can be effectively employed from a moving platform, in this instance, the Research Vessel ACANIA. Further, a high-speed digital processing system has been added to allow simultaneous real time digital analysis of 20 harmonics of a sawtooth waveform.

A brief and simple description of the experiment sets the scene for detailed discussion of each facet of the project. An underwater test assembly was suspended from the Research Vessel ACANIA's fantail hydraulic crane. The test rack was lowered to a depth of 15.2 meters, a depth determined from previous research to be bubble-free [Medwin et al., 1975]. Test rack depth was determined by pulsing through an upward looking transducer. This pulse was reflected from the surface and received on either of the hydrophone receivers mounted on the test rack. By triggering an oscilloscope on the transmitted pulse, the time required to reach the hydrophone was displayed on the CRT. This time was then halved to give one-way travel time and converted to depth by multiplication with the nominal 1500 meters/sec speed of sound through sea water.

When signal processing was accomplished by digital methods, a continuous sawtooth waveform, rich in harmonic content, at a fundamental frequency of 5 kHz, was transmitted into the water. This sound wave was directed past two fixed hydrophones approximately one meter apart. Figure 2 shows the CRT display of this transmitted signal along with the received signals after amplification and filtration. The amplified and filtered outputs of these hydrophones were sampled with an analog/digital converter and fed to a high-speed digital computer. This signal processor computed and displayed the attenuation as well as the fractional phase differential between the two hydrophones.

When analog methods were used to obtain data, pure sinusoidal waveforms were transmitted into the ocean. The returning signals after amplification and filtration, were passed to a vacuum-tube voltmeter for amplitude measurement and to a phasemeter for relative phase measurement.

The 15.2 meter depth run was, then, a calibration run. As the test rack was raised closer to the surface and additional runs were made, the excess attenuation and phase shift above that measured at 15.2 meters could be attributed to resonant bubbles present in the sound field. Application of the theory discussed in Section I-C of this thesis permits computation of bubble populations as a function of size and depth. Further application of theory contained in

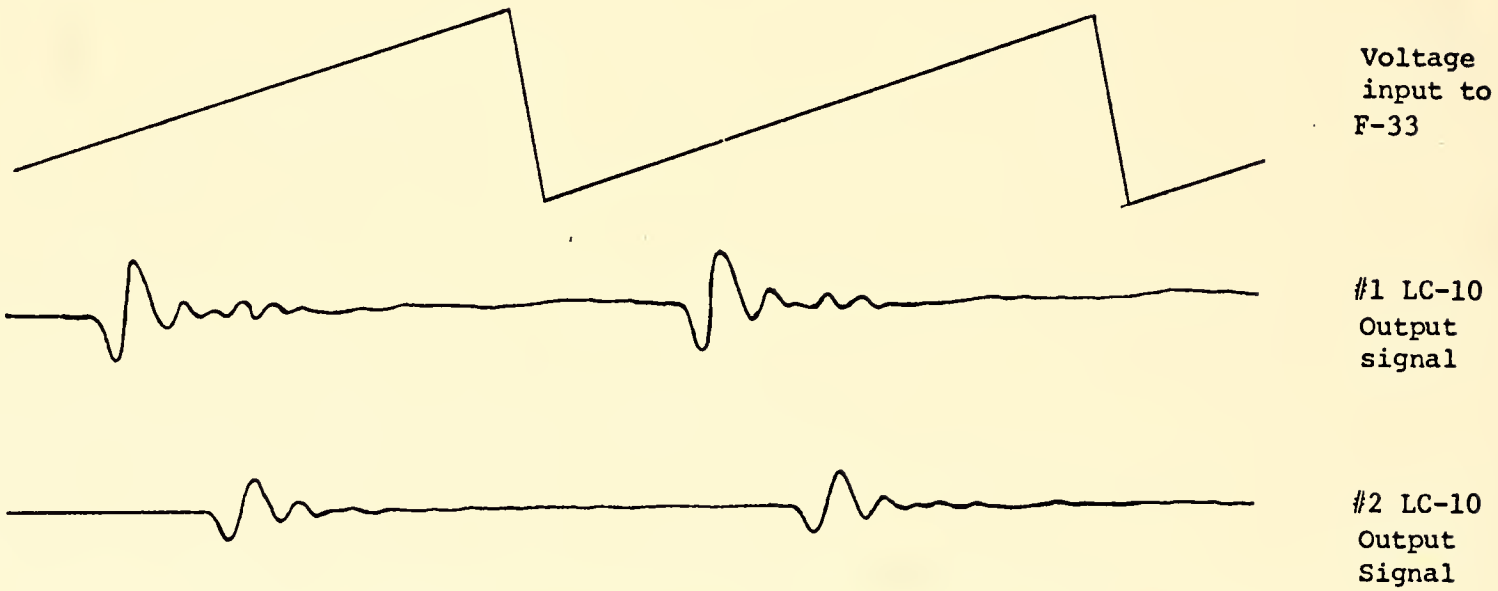

FIG. 2 TRANSMITTED WAVEFORM AND FILTERED RECEIVED SIGNALS

Section I-E enables caluclation of the change in speed and sound directly attributable to the presence of these resonant bubbles.

III. UNDERWATER EQUIPMENT

A. SOURCE TRANSDUCER

The source was the USRD F-33 directional transducer designed for operation from 1 kHz to 150 kHz. It has two arrays, an inner array of lead zirconate-lead titanate ceramic elements measuring 1.5" by 2.0", and an outer array of barium titanate ceramic elements measuring 8.0" by 8.5". These dimensions result in a far field, a^2/λ, of 0.76 meters from the transducer face at 100 kHz. The transducer is designed to take a maximum voltage input of 200 volts (rms). The typical transmitting response ranges from a pressure of 17 dB re 1 ubar/volt at 5 kHz to 48 dB re 1 ubar/volt at 100 kHz. These values are computed for a distance of one meter and assume 100 feet of attached cable.

B. RECEIVING ELEMENTS

The hydrophones chosen were Atlantic Research Corp. Model LC-10s. These hydrophones exhibit a flat frequency response over the frequency range 1 kHz to 100 kHz with a voltage sensitivity in the vicinity of -108 dB re 1 volt/ubar. The sensing element is of lead zirconate titanate encased in a bonded neoprene sheath 1.13 inches in length and 0.38 inches in diameter. The element is then connected by six feet of low noise cable to a Model 2010 NUS 30 dB preamplifier encased in a sealed, waterproof can. This

preamplifier has a gain accuracy ±0.2 dB at 1 kHz, is usable to 200 kHz, and is powered by 12 volts DC at 4.5 milliamps.

When transmitting in the pulse mode to check for frame reflections, a definite pulse was seen on the receiving equipment with no phase lag from the transmitted signal. This proved to be an electromagnetic field that was generated simultaneously with the sound generation. Acoustic signal to electromagnetic noise ratios were found at all frequencies of interest, and showed this noise to be more than 30 dB down from acoustic signal levels. Geometric phasor diagrams at one hydrophone showed this to be the equivalent to an error of ±3.2% in attenuation when the signals were in phase or 180° out of phase. The phase angle effect was most pronounced when the phasors were 90° out of phase, causing an angular error of ±1.8°. If the signal, in traveling to the second hydrophone, should have a similar relation but in the other direction, the combined effects would be 6.4% attenuation error and 3.6° phase error. The phase angle changes caused by variations in the speed of sound during a normal experimental run were sufficiently small that most of this error would have canceled out in the subtraction of the calibration run data, making the expected errors acceptably small.

When transmitting a sawtooth continuous waveform, however, a very significant electromagnetic signal was transmitted at each sharp change in voltage direction. Since it was impossible to accurately determine which

harmonic frequencies were contained in this signal, no meaningful signal to electromagnetic noise ratios could be calculated, and it became necessary to eliminate the radiation altogether, or reduce it to 30 dB below the smallest harmonic component received. The received electromagnetic signal was finally reduced to undetectable magnitudes by completely shielding the LC-10 hydrophone and transmitting cable from the sensing element to the preamplifiers. This shielding was done with copper mesh braided shielding which was grounded to the preamplifier casing. This shielding was then insulated from the water with neoprene and tape, and the sensing element was insulated with a coating of epoxy. The sensitivity loss caused by this shielding was approximately 3 dB, but since it was constant under all sampling conditions, it also canceled out in subtraction of the calibration run. A previous design, using neoprene for covering the sensing element showed evidence of bubble entrapment. This was avoided by using epoxy which had been heated and degassed by pumping prior to application to the sensing element.

C. SUPPORT FRAME

The initial design of the underwater test rack was taken from previous thesis work with minor modifications. Figure 3 shows, in schematic form, this test assembly with all modifications made during test and development. The frame was constructed of 1-1/4" hollow steel pipe. In

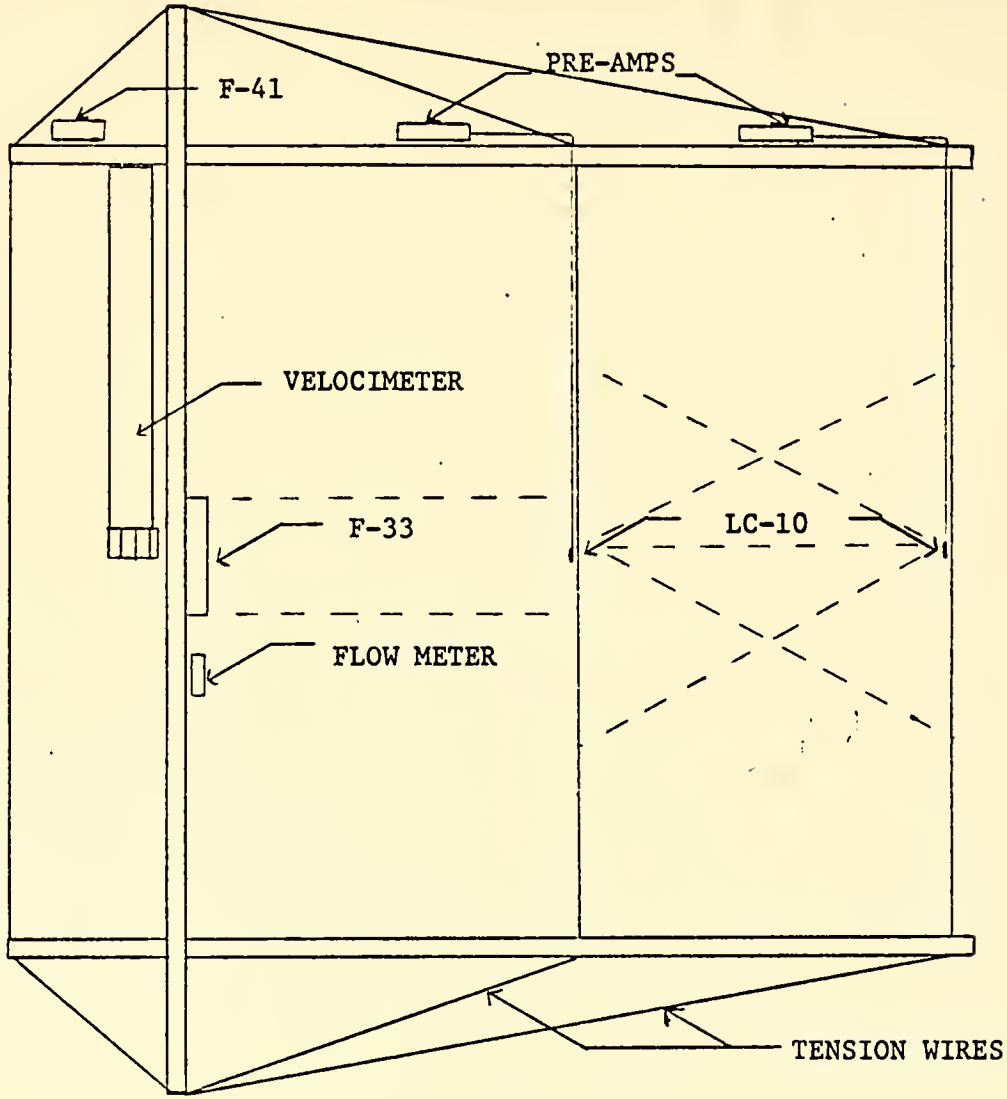

FIG. 3 . UNDERWATER TEST RACK AND ASSEMBLY MODEL I

order to minimize frame reflectivity, the pipe frame was sleeved with heat-shrunk rubber and silicon rubber wedges were built up inboard on the horizontal arms of the frame. The source transducer was mounted midway on the vertical frame member. Heavy duty nylon shotline supports drawn between rubber shock mounts were affixed parallel to the vertical frame member, designed to support the passive hydrophone elements. Sealed cans containing preamplifiers for these hydrophones were mounted outboard on the upper horizontal frame member far back of the sound field. An upward looking transducer was mounted behind these pre-amplifiers to be used to determine depth. On the underside of the upper arm, a current probe was mounted for remote monitoring of the water flow past the test assembly. Finally, the reference velocimeter was mounted in the vertical position and suspended from the upper horizontal extension behind the source transducer.

Fully assembled, with all equipment mounted in place, this test assembly weighed approximately 150 pounds. Figure 4 shows this test assembly with all supporting equipment in place.

From previous research work, it was known that to obtain acceptable accuracy both in amplitude and phase, it was necessary to reduce frame reflections to a level 30 dB below the direct path amplitude. The test assembly, less velocimeter, was lowered into a fresh water anechoic laboratory tank for determination of reflection magnitudes.

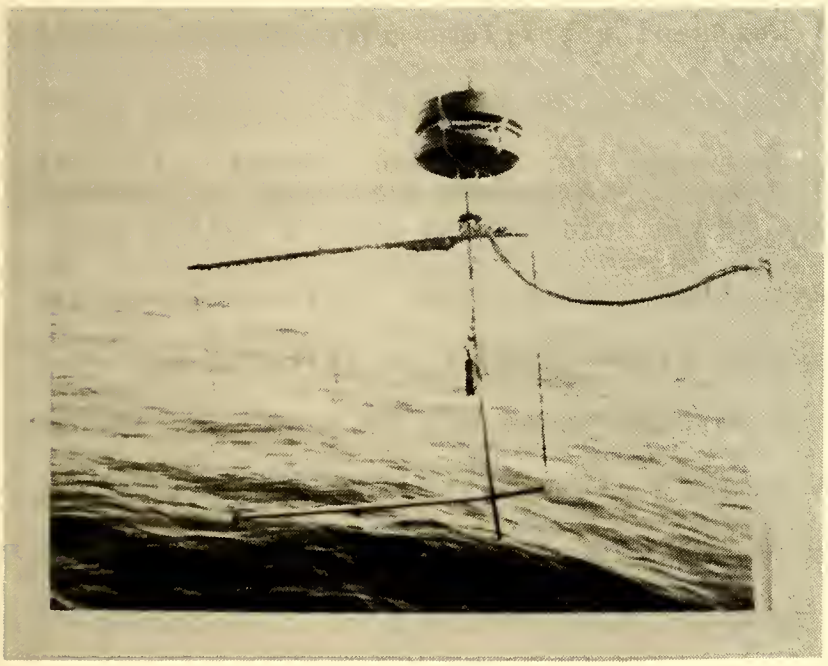

FIG. 4 RACK MODEL I WITH SUPPORTING EQUIPMENT

This testing was done using a gated pulse. By carefully measuring both direct and specular reflection path lengths, and measuring the relative amplitudes of the direct and reflected received signals on an oscilloscope, it was possible to identify each of the path contributions uniquely based upon travel time along the path. As was true with electromagnetic radiation contributions, this -30 dB high limit on reflection amplitudes resulted in a maximum attenuation error of 6.4% and a maximum phase differential error of 3.6°. Again, however, the small temperature differences between the 50 foot calibration depth and the upper ocean depths of interest ensured the speed of sound and therefore the acoustic wavelength would change by such a small amount that most of the error induced by reflections would cancel out in subtraction. The goal of 30 dB direct signal to reflected signal ratio was attained at all frequencies of interest on this original test assembly.

First attempts to use this test assembly configuration at sea were totally unsuccessful. Motion of the apparatus through the sea imparted by the floating platform caused instability problems. Transient noise signals injected by snapping of the primary rack support cable totally obliterated the received signal. Apparent relative movement and vibration of the hydrophone support lines added to this instability both in amplitude and phase. Attempts to minimize these problems by mounting flexible wire strong-backs to the assembly for frame stability and

adding a fine horizontal support line between the hydrophone elements to reduce relative movement met with only partial success. The test assembly remained unsatisfactory with each of these modifications. Due to the nature of the difficulties encountered, it did not appear feasible to further modify this test rack design with any expected degree of success. The obvious design requirements indicated the need for a more stable test vehicle.

The problem of support frame stability was confronted first. It appeared most desirable to increase the rigidity of the design. In making a more rigid and compact frame, reflectivity loomed as the largest obstacle. Not only would the added surface area of the reflector and its closer proximity to the sound field cause difficulties, but the pulsation method of determining reflective contributions would be unusable because of the small differential in path length and hence signal travel time. It was decided that this problem could be circumvented by making use of the 15.2 meter bubble-free calibration run. It was hoped that in computing the excess attenuation at the upper ocean depths by subtracting out the reference attenuation at 15.2 meters, reflective contributions could be lost in cancellation.

Figure 5 shows schematically the structure of test assembly Model II. All support equipment previously used on rack Model I was adapted for use on assembly Model II. Longitudinal construction was 2-3/8" PVC pipe. Mounting

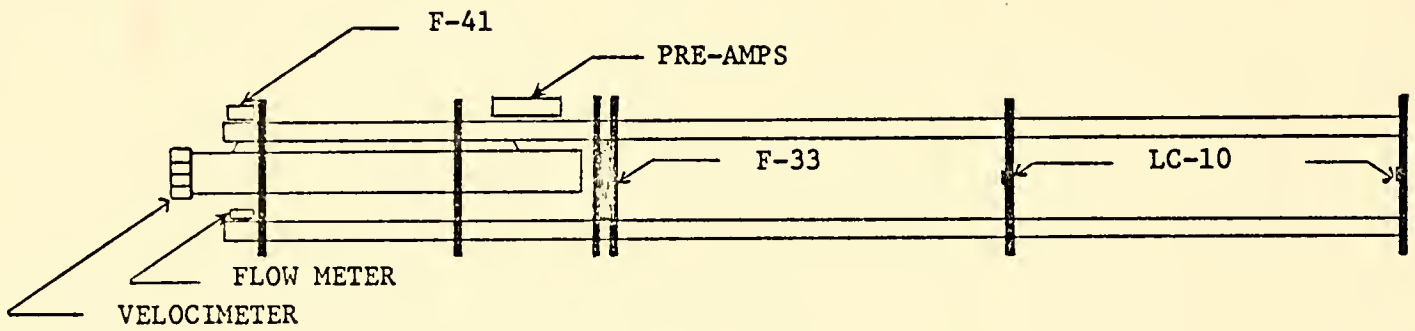

FIG. 5 UNDERWATER TEST RACK AND ASSEMBLY MODEL II

brackets for the source transducer and the reference velocimeter were made of 3/8" aluminum. Mounting brackets for hydrophone element supports were of 1" lucite. These support brackets further provided frame rigidity. Total weight of the fully-rigged test assembly was approximately 150 pounds.

In spite of the superior performance of assembly Model II as regards signal stability and frame rigidity, analysis of at-sea data indicated that reflective interference from Model II was indeed excessive. Assembly Model I was employed for the remainder of the research work. Nylon fish line under slight tension (dashed lines in Figure 3) was added between the hydrophone support lines in an attempt to minimize relative movement. Additional fish line was used between the frame and the support lines for vibration damping. Cushioning was added between the preamplifier canisters and the support frame to eliminate vibration transmission. These devices helped somewhat; however, the assembly Model I still was usable only in relatively mild sea and weather conditions, and there was continuing evidence of incorrect phase measurements at the lower harmonics of the fundamental sawtooth frequency. Finally, stuffing the tubes with steel wool for vibration damping made the assembly usable in moderately heavy sea conditions.

D. SHIP MOTION ISOLATION EQUIPMENT

The next problem was to minimize the transient signals imparted to the rack by the main support cable. The solution was to minimize the submerged weight and to support the test assembly from a non-linear elastic support line creating a simple harmonic oscillator with a period which would be relatively uninfluenced by the motion imparted to the ship by passing waves.

A 20-foot section of one-quarter inch cotton-impregnated elastic cord was obtained, which had a low constant of elasticity (s = force/distance) of 0.029 lbs/inch when the applied force was approximately five pounds. This corresponds to a resonant frequency ($\omega_n = \sqrt{s/m}$) of 0.273 rad/sec and a period of 23 seconds assuming an assembly mass of 150/g slugs. For all ocean swell waves of period about 11 seconds, the system was relatively unaffected by passing waves.

To achieve the five pound weight necessary to arrive at this low resonance frequency, a method of flotation was necessary. This flotation device was required to achieve a negative buoyancy of five pounds when the test assembly was submerged at various depths. This device had the further advantage of increasing the mass of the assembly thereby increasing the natural period of oscillation as well as providing a damping effect that further isolated the assembly from surface motion.

A cylindrical container, open at one end, was constructed of aluminum and was filled with varying amounts of styrofoam in an attempt to obtain the desired buoyancy. The compressability of the styrofoam made this an unusable design for the multitude of depths to be investigated.

In order to provide a constant buoyancy at varying depths, a second device was constructed using an air bladder which was connected to an air supply on board the ship by a flexible air hose. This bladder, which consisted of an inner tube within a tire for protection, but open to the water, was connected to another fully inflated tire mounted on a rim, which acted as a fixed size buoyant device as well as a damper. The air pressure in the fully inflated tire was kept in excess of the depth pressure anticipated to preclude its compression in size. The pressure in the bladder was always apprxoimately that of the surrounding medium, and increased with depth. Since a constant displacement was needed, air had to be added with increased depth.

Figure 6 shows a sketch of the flotation device in position above rack Model II.

E. DEPTH DETERMINATION

The transducer selected for depth determination was the USRD Type F-41 directional transducer designed for use from 15 kHz to 150 kHz. The transducer is composed of an

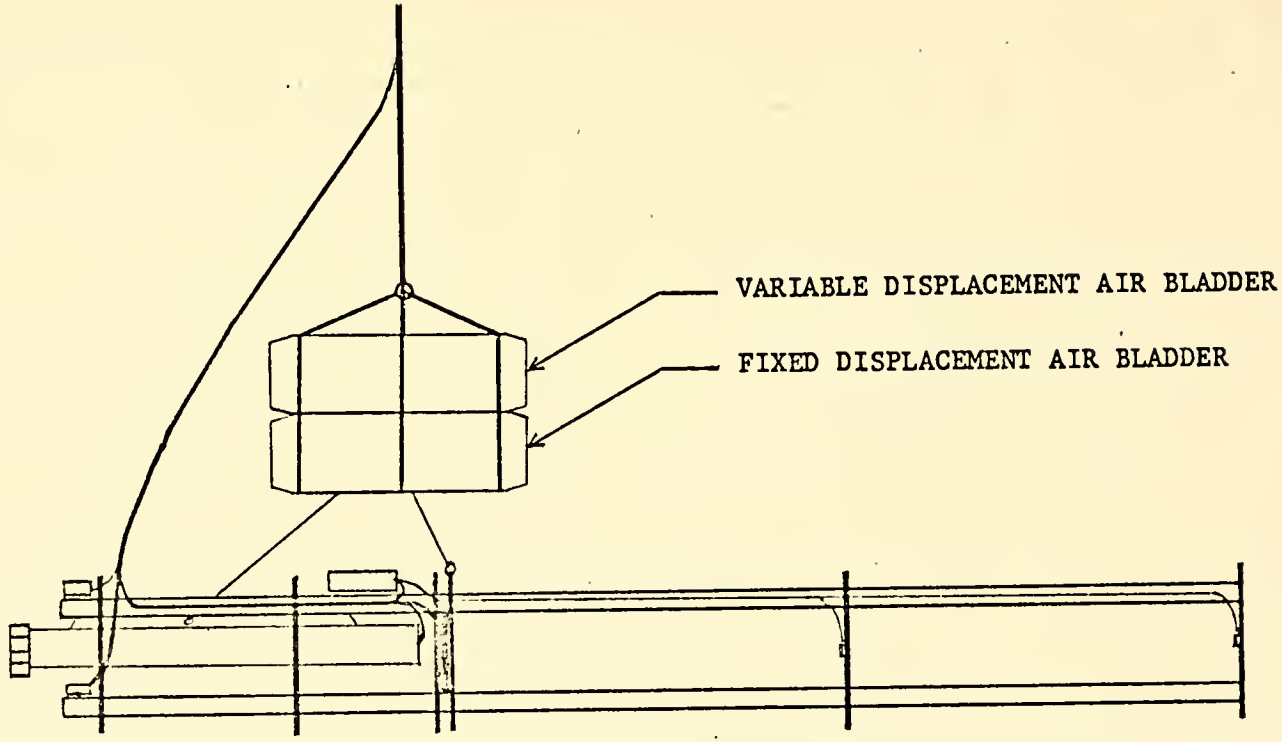

FIG. 6 FLOTATION DEVICE AND RACK MODEL II

array of lead zirconate-lead titanate ceramic elements measuring 1.5" by 2.0" that will operate at input voltage up to 200 volts (rms). A typical transmitting response shows a pressure of 60 dB re 1 ubar/volt at 150 kHz. This is computed for a distance of one meter from the transducer face and assumes a 100 foot cable.

F. CURRENT FLOW METER

Although not necessary as a data input to final numerical analysis, a Marsh-McBirney Model 711 Electromagnetic Water Current Meter was mounted on the test rack to provide oceanographic background for the experiment. This device measures water flow in two directions orthogonal to the longitudinal axis of the instrument probe. Maximum measurable flow is ±10 ft/sec. Accuracy is to within ±2% of the reading.

G. REFERENCE VELOCIMETER

Finally, the velocimeter used to determine the reference speed of sound for investigation of the change in speed of sound due to resonant bubbles was the NUS Model 1630-002 SV/T/D sensor. This unit determines sound velocity, temperature, and depth. The per cent of error in depth readings for the shallow waters of interest rendered this section of the instrument useless. The sound velocity module gave accuracy to ±0.15 meters/sec. The temperature module was accurate to 0.1° C.

IV. SHIPBOARD/LABORATORY EQUIPMENT

Several electronic devices were used in various configurations depending on the information to be obtained. All equipment used will be described, followed by a description of the set-ups for each experimental arrangement.

A. SIGNAL GENERATING EQUIPMENT

To generate a monofrequency signal for the upward looking sonar, and for precise triggering of the sawtooth function generator, a General Radio Model 1162A Frequency synthesizer was used. This provided a highly stable sine wave with a maximum output voltage of 2 volts (rms). Frequency synthesizing was accomplished with a quartz crystal oscillator. The frequency was digitally selectable to 1 MHz with accuracy to 0.01 Hz.

To generate a monofrequency pulse for determining depth, or measuring reflected sound and electromagnetic radiation, the synthesizer wave form was gated through a General Radio 1396-A tone-Burst Generator. This generator permitted the signal to pass or not pass depending on the selected number of cycles to be counted.

To generate a sawtooth waveform for the transducer, the synthesizer was used to trigger a Wavetek 144 Sweep Generator. The experiment consistently used a 5 kHz triangular waveform with a 19:1 asymmetry as an approximation of a sawtooth wave.

After generation, the output voltage was amplified by a Hewlett-Packard 467A Power Amplifier to a maximum of ±20 volts (peak) before being passed to the appropriate transducer.

A Fluke 8000A digital multimeter was used to insure precise amplitudes of transmitted voltages.

B. SIGNAL PROCESSING EQUIPMENT

All signals were received by the LC-10 hydrophones and amplified by the 30 dB NUS preamplifiers as described in Section III-B. They were then transmitted through 150 feet of shielded cable to the ship where they were evaluated.

The received signals were immediately filtered to reduce low frequency motion-induced and ambient noise, and to prevent high frequency aliasing as discussed in Section V-A. The filtration was done using Krohn-Hite 3550(R) filters with a bandpass adjustable to any bandwidth, and a range between 2 Hz and 200 kHz, with a roll-off at both the high-pass and low-pass frequencies of 24 dB/octave. These generated less than 200 microvolts of noise and could handle a signal up to ±7 volts (peak).

The filtered signals were further amplified by a pair of Princeton Applied Research (PAR) 113 Low Noise Preamplifiers which could amplify signals with frequency components up to 300 kHz with an input of up to 1 volt (rms). The maximum output possible was 10 volts (peak-to-peak) with an expected distortion less than 0.01%. The bandpass was set

at DC/300 kHz throughout the experiment, thereby rendering the feature ineffective in comparison to the Krohn-Hite 3550(R) filters. An oscilloscope overlay of the input and reduced output of these amplifiers showed all frequency components to be equally amplified, with no visible distortion.

When determining depth, frame reflection, and electromagnetic field radiation, the transmitted pulse and received signal were displayed on a Tektronix 545B Oscilloscope, triggered by the transmitted pulse, to determine elapsed time of travel or amplitude of the respective signals.

The velocimeter, described in Section III-G, sent a frequency signal through 150 feet of coaxial cable to a NUS 3010-101 Signal Conditioner and an NUS 7450-101 F-V Converter with an associated power supply. These provided frequency sampling terminals for sound velocity, temperature, and depth. These frequencies were converted into the values desired by substituting them into calibration formulas provided. The sound velocity obtained by these formulas was accurate to within ±0.15 meters/sec, the temperature to within ±0.1° C.

If signal processing was to be done by digital methods, the filtered and amplified signals were next sampled by a pair of Phoenix ADC 712 analog to digital converters with a sampling rate up to 350,000 samples per second. The 12 bit quantization contributes an error of 1/4095 times the maximum voltage sampled within each frequency component.

The least power is generated in the 5000 Hz frequency component, with an average peak voltage of .050 volts. The error is then 1.22×10^{-5} volts which yields a maximum attenuation error between the two hydrophones of $20 \text{ Log}_{10}[(V_{5kHz} + V_{error})/(V_{5kHz} - V_{error})]$ or .0042 dB. Since the attenuation is calculated by subtracting a calibration run from each run in an inhomogeneous medium, the maximum possible quantization error is doubled, or .0084 dB. Because this error is random, and since 2048 samples were taken each run, the probable error is much less than this value. The phase angle is also in error because of this quantization. The same frequency component yields a real and an imaginary voltage component from which a phase angle is computed. The error expected from these values is $\text{Tan}^{-1}[(V_{imag} + V_{error})/(V_{real} - V_{error})] - \text{Tan}^{-1}[V_{imag}/V_{real}]$ which is a maximum when $V_{imag} = 0$, giving a value of .014 degrees.

The digitized signal was processed finally through an Interdata 70 Digital Computer which analyzed the received signals as described in Section V-A.

If signal processing was to be done by analog methods, the filtered and amplified signals were fed, separately, to a Hewlett-Packard 400D Vacuum-tube voltmeter and the individual voltage levels were recorded and compared. The HP 400D is an accurate average-responding rms voltmeter which will measure AC voltages from 0.001 volts full scale

to 300 volts full scale over a frequency range from 10 Hz to 4 MHz. The signals were then sent to a Dranetz Model 305 Phasemeter manufactured by Engineering Laboratories, Incorporated. This device displayed the phase differential between signals received by the two hydrophones. The Model 305 Phasemeter operates with input voltages from 10 millivolts to 50 volts (rms) and is accurate to ±0.25°.

Equipment set-ups for the various experimental configurations are shown schematically in Figures 7, 8, and 9.

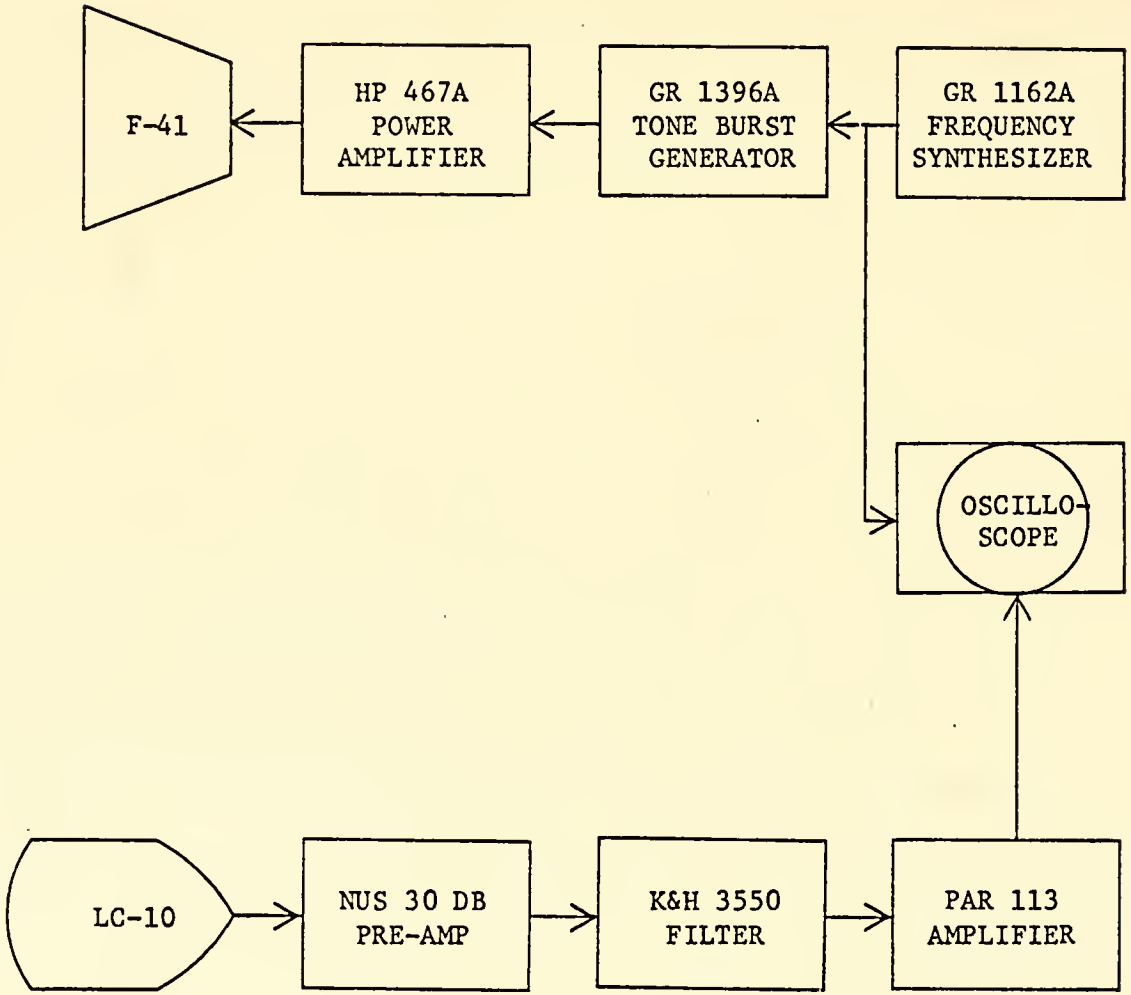

FIG. 7 EQUIPMENT SET-UP FOR DEPTH DETERMINATION

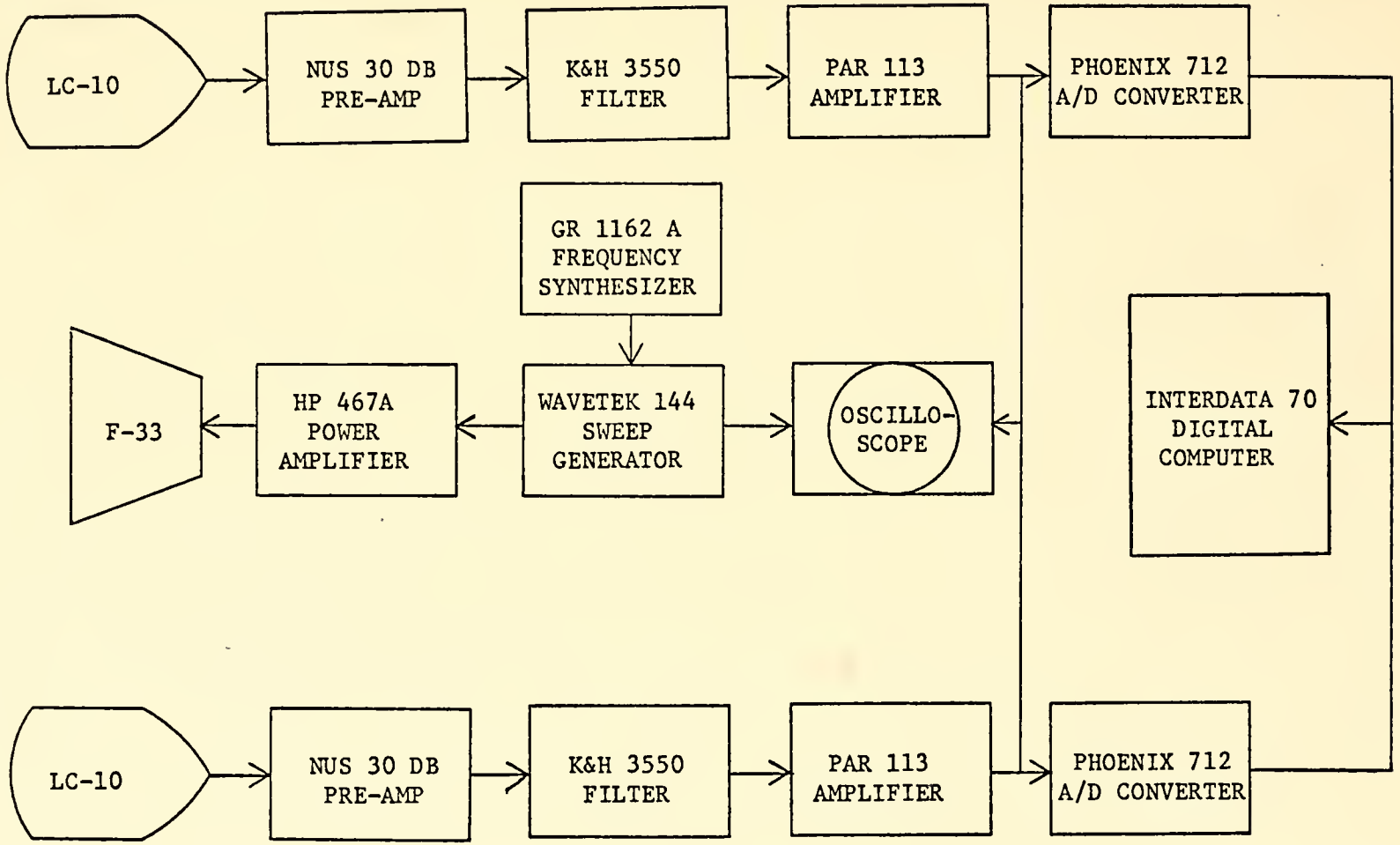

FIG. 8 EQUIPMENT SET-UP FOR DIGITAL SAMPLING

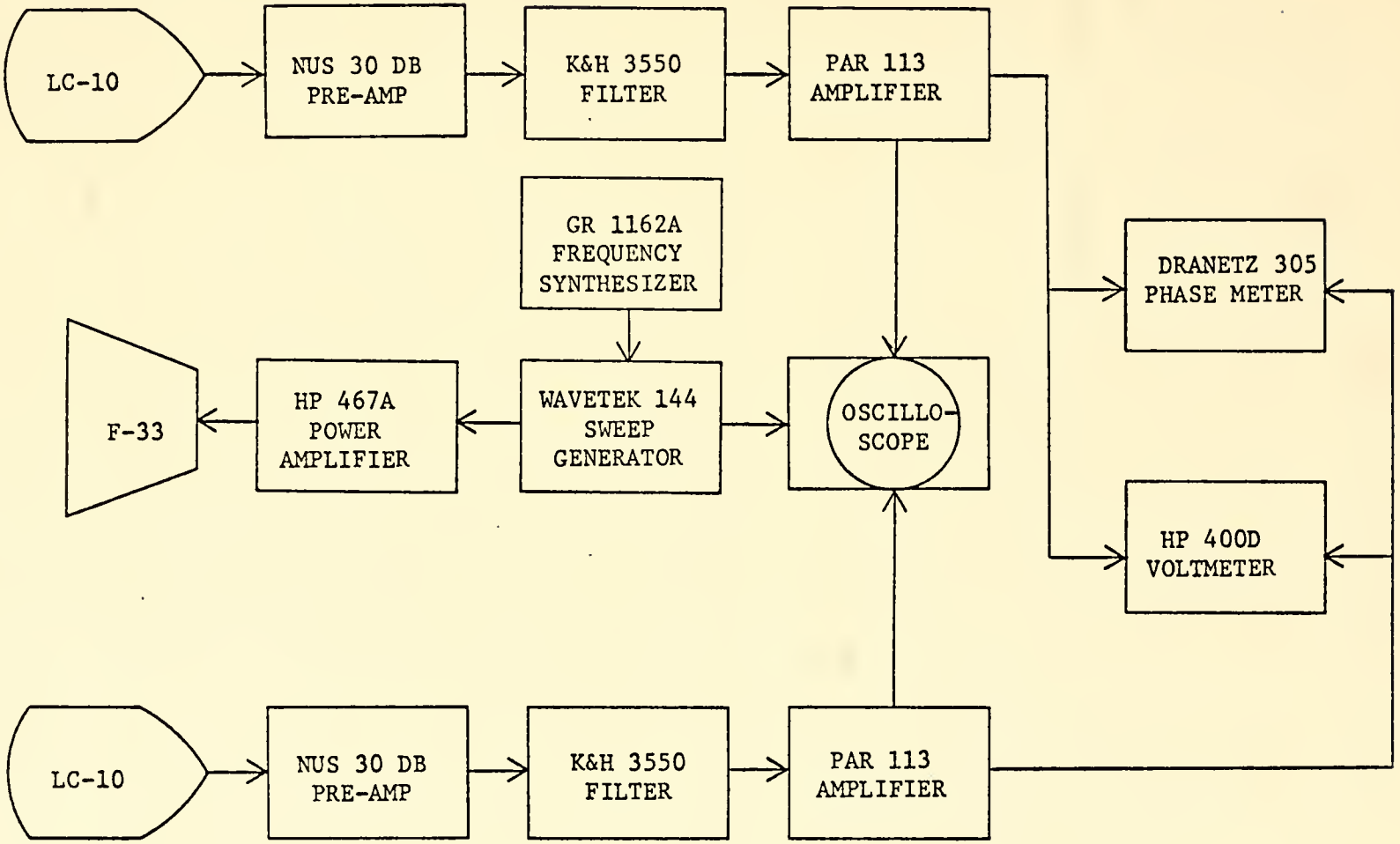

FIG. 9 EQUIPMENT SET-UP FOR ANALOG SAMPLING

V. SIGNAL PROCESSING

A. DIGITAL PROCESSING

Previous research along these lines has been limited by the time requirements to change frequencies, change filters, and take amplitude and phase angle measurements at each frequency of interest. This required hours for a single series of readings before investigating other depths. The use of a high speed Interdata 70 Digital Computer permitted this series to be sampled and displayed in less than three minutes using the technique of the Fast Fourier Transform (FFT).

The 500 Hz sawtooth waveform sent to the transducer can be considered to be composed of the sum of all sinusoidal harmonics of 500 Hz. The amplitudes decrease as the harmonics increase and there is a fixed phase angle relationship for each harmonic relative to the fundamental frequency. For example, the Fourier series representation of a triangular wave with a 4:1 asymmetry is

$$f(x) = \frac{32}{3\pi^2} \sum_{1}^{\infty} \frac{1}{N^2} \operatorname{Sin} \frac{N\pi}{3} \operatorname{Sin} \frac{N\pi t}{L} \qquad (27)$$

where 2L is the wavelength and t is the time along the repetitive waveform.

A piston transducer does not transmit all frequencies with equal power response or with the same acoustic

radiation pattern. Therefore, the signal received by the hydrophones is already considerably changed in form from a sawtooth wave, with low frequencies suppressed, and high frequencies unevenly attenuated by the water. The response of the LC-10 hydrophones further suppresses the high frequencies, and finally, the Krohn-Hite filters remove all frequencies below 1 kHz and above 100 kHz. Figure 2, page 32, shows the transmitted signal and filtered responses.

This filtered, sampled signal is sent into the computer where a Fast Fourier Transform is performed. The FFT is a digital algorithm which converts the sampled waveform into the power contained within each frequency component and, unlike analog wave analyzers, preserves the phase relation between each frequency component and the fundamental harmonic. The computer displays a power spectral density and associated phase angle for each of the two hydrophones and computes and displays attenuation and phase angle difference between each hydrophone. Appendix A shows a sample computer output generated from a contrived experimental run. When these results for a bubbly medium are compared with those for a bubble-free medium as expected at the 50 foot calibration depth, the change in sound speed and excess attenuation caused by resonant bubbles can be caluclated as described in Sections I-C and I-D.

The two most common problems encountered with the FFT are aliasing and windowing effects. Aliasing is the property of the FFT whereby power in harmonics with a frequency higher than one-half the frequency of sampling (Nyquist sampling rate) is combined with frequencies below this maximum displayed Nyquist frequency. To avoid this, we sampled the waveform at 320 kHz which permitted a display of frequencies up to 160 kHz, and we filtered out frequencies above 100 kHz. The windowing effect is caused by the requirement for a Fourier Transform that the signal be sampled over a time extending from minus infinity to plus infinity. The FFT can be considered to take the sampled waveform in its finite time "window," mathematically project it into all preceding and subsequent time windows over all time, and then compute its Fourier Transform. Any discontinuities or radical changes in direction at the junction of these "windows" causes a mathematically generated series of false harmonics. This results in the convolution of the waveform sampled with a pulse having the duration of that window, or, in the frequency domain, this is the multiplication of each harmonic impulse spike with a sinc function. This pitfall was avoided by sampling the signal at a harmonic of the generated signal thereby avoiding discontinuities and obviating the need for a hanning or hamming function.

The 1024 sampling points permitted the FFT to compute 512 power spectral density lines, equally divided into

the 160 kHz maximum frequency permitted by the Nyquist sampling theorem. Each power spectral density line therefore represented a bandwidth of 312.5 Hz. The program permitted any selected frequencies to be displayed. A display of all spectral density lines, once with the signal projecting into the sound field and once with the receivers in the presence of ambient noise only, gave a good measure of the signal to noise ratio at each harmonic. Ratios in excess of 60 dB in the middle frequencies (35-80 kHz) could be obtained, and ratios greater than 40 dB existed throughout the spectrum.

B. ANALOG PROCESSING

Analog processing was used to verify the accuracy of the values obtained digitally, and also was used exclusively on those days when the computer would not operate on ship's power.

Using the set-up described in Section IV-B, and shown in Figure 9, a monofrequency signal at each frequency of interest (5 kHz, 10 kHz, etc.) was transmitted through the F-33 transducer. A 40 volt (peak-to-peak) signal was used for frequencies below 80 kHz. To prevent distorting the transmitted signal, this was reduced to 20 volts for higher frequencies.

The received signal was bandpassed to approximately 1/10 octave, centered on the transmitted frequency, by the K&H 3550 filters. In order to maintain sufficient voltage

to drive the phase meter, signals below 25 kHz were amplified by a factor of 20, those between 25 kHz and 35 kHz by a factor of 10, and no amplification was used for frequencies above 35 kHz.

The amplitude of each signal was read from the HP 400D vacuum tube voltmeter in decibels re 1 milliwatt at 600 ohms, and the attenuation was obtained by subtracting the two measurements. Bubble populations were then calculated as described in Section I-C.

The phase difference was read directly from the Dranetz 305 phase meter, permitting sound speed calculations as described in Section I-D.

VI. EXPERIMENTAL RESULTS

A. RESULTS AT ANCHOR IN MONTEREY BAY

The first successful at-sea experiment was run on 12 and 13 November 1974 in Monterey Bay, Lat. 36-37.7N, Long. 121-54.1W, in 38 meters of water, well removed from any sewage outflow or any noticeable singularities. Calm seas with swell height averaging 0.5 meters and wind speed averaging 3.5 knots, prevailed throughout the 18 hours of the experiment. Specific weather and sea conditions were recorded hourly to permit comparison with observed fluctuations. These data are tabulated in Appendix A. In-situ sound speed, temperature, and flow rates for each run are tabulated in Appendix B.

1. Procedure

A 5 kHz sawtooth waveform of 30 volts peak-to-peak was applied to the F-33 transducer mounted on model I rack. Because the source has an output that is more efficient at mid-range frequencies, the power spectral density was not uniform across the frequency range of interest. Figure 10 shows the sound pressure levels received at the closest hydrophone for each harmonic component of the generated signal. The received signals were amplified by 30 dB, bandpass filtered between 1 kHz and 100 kHz, then amplified an additional 20 dB, giving a maximum peak-to-peak signal of about five volts. See Figure 8 for a schematic drawing of the equipment set-up.

FIG. 10 SPECTRAL OUTPUT OF F-33TRANSDUCER WITH 5 KHZ
APPLIED SAWTOOTH WAVEFORM OF 30 VOLTS (PEAK-TO-PEAK)
Sound level measured at 1 meter from source

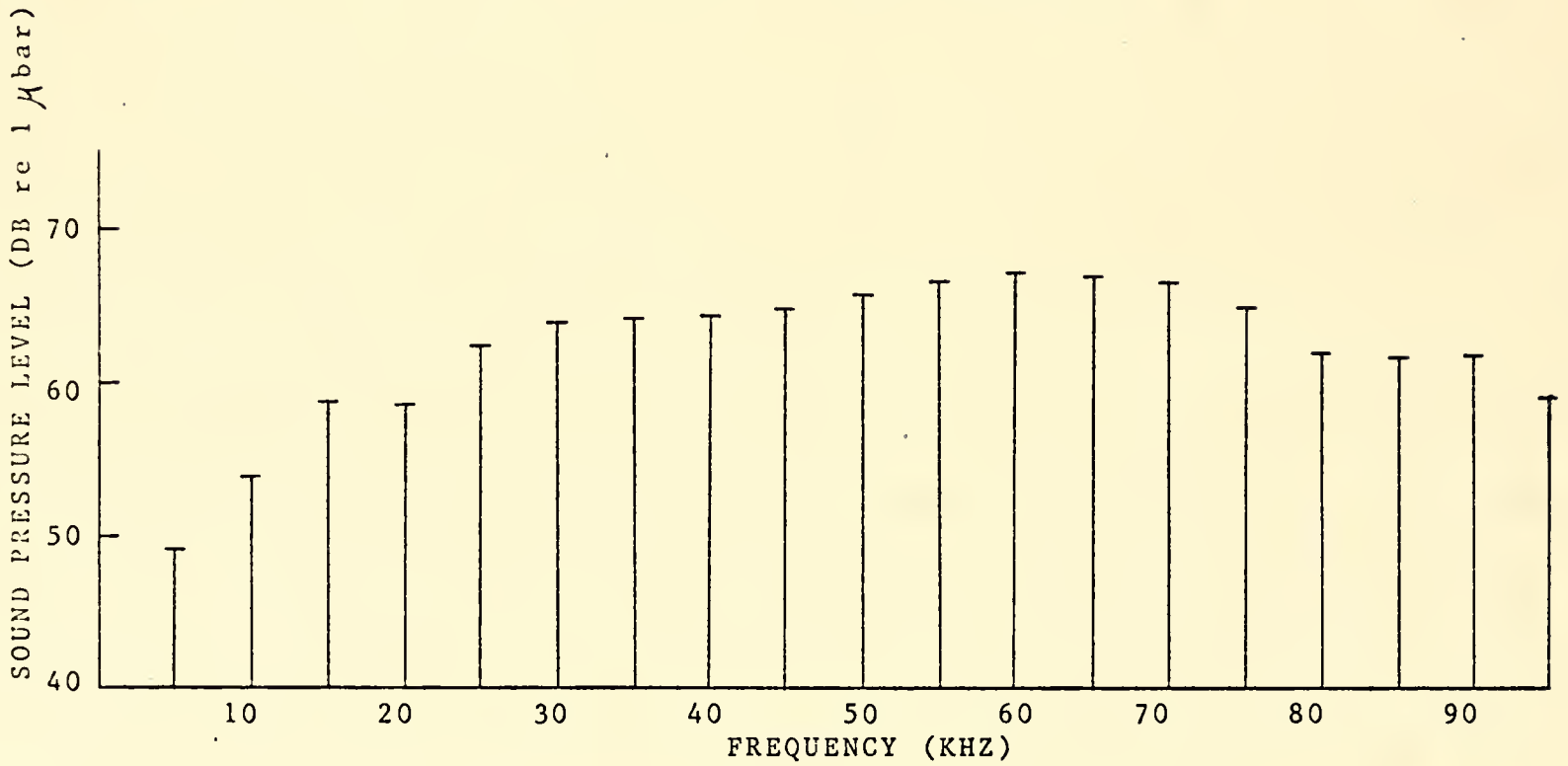

Two types of runs were made concurrently. One was an 18-hour series of runs at a constant depth of five meters, taken every other hour. The other type included two series of runs at 3, 5, 8, and 10 meters, and a reference run at 15.2 meters, taken at 1630, 12 November and 0800, 13 November. At each depth, five or more sets of samples were taken in a total time of about 15 minutes. These were later used to provide an average value and a standard deviation. Representative runs from the 18-hour series are included in this analysis as are each of the two variable depth series.

2. Amplitude Attenuation

Attenuation data obtained during the 12-13 November at-sea experiment disproved an initial assumption important to our experimental analysis. The 15.2 meter depth, previously determined to be relatively bubble-free in research conducted at NUC, San Diego, and Bass Strait, Australia, was found to have significant bubble populations at this location. Data analysis indicated that attenuations at this depth often exceeded attenuations at near-surface depths. Thus, there was no bubble-free reference from which to find excess attenuation at upper depths. It was decided to extract from the data the minimum dB difference recorded at each harmonic frequency regardless of time or depth and to use these values as the dB difference between the two hydrophones for a zero

attenuation medium. The computed bubble populations, then, are not referenced to an absolute zero bubble population but to a nominally bubble-free medium.

Figures 11, 12, and 13 show graphically the number of bubbles in a one micron band calculated to exist in a cubic meter of water during this at-sea run. The shape and scope of these figures is remarkably similar. Populations of small radius bubbles below 50 microns varied as R^{-4}. Larger sized bubbles above 50 microns varied as $R^{-2.4}$. Some vertical stratification was apparent with more bubbles at shallower depths. However, this stratification trend was slight and did not consistently hold for all radii. Figures 11 and 12 depict the 1630 12 November and 0800 13 November variable-depth series. Figure 13, the 18-hour survey at five meters depth, also shows only slight change over the observation period. However, there is slight evidence of more bubbles in the hours of darkness than daylight.

Figures 14, 15, and 16 show both excess attenuation and the fractional volume of air for a one micron radial increment contained in resonant bubbles plotted as a function of frequency. In all three figures, a strong peak occurs at 15 kHz indicating a marked attenuation caused by bubbles resonant at this frequency. This frequency maximum translates to a bubble radius between 250-350 microns. Later peaks appear to vary between 30 kHz and 40 kHz, corresponding to bubble radii between 90 and 170 microns.

FIG. 11 ATTENUATION-DERIVED BUBBLE POPULATIONS AS A FUNCTION OF BUBBLE RADIUS IN MONTEREY BAY

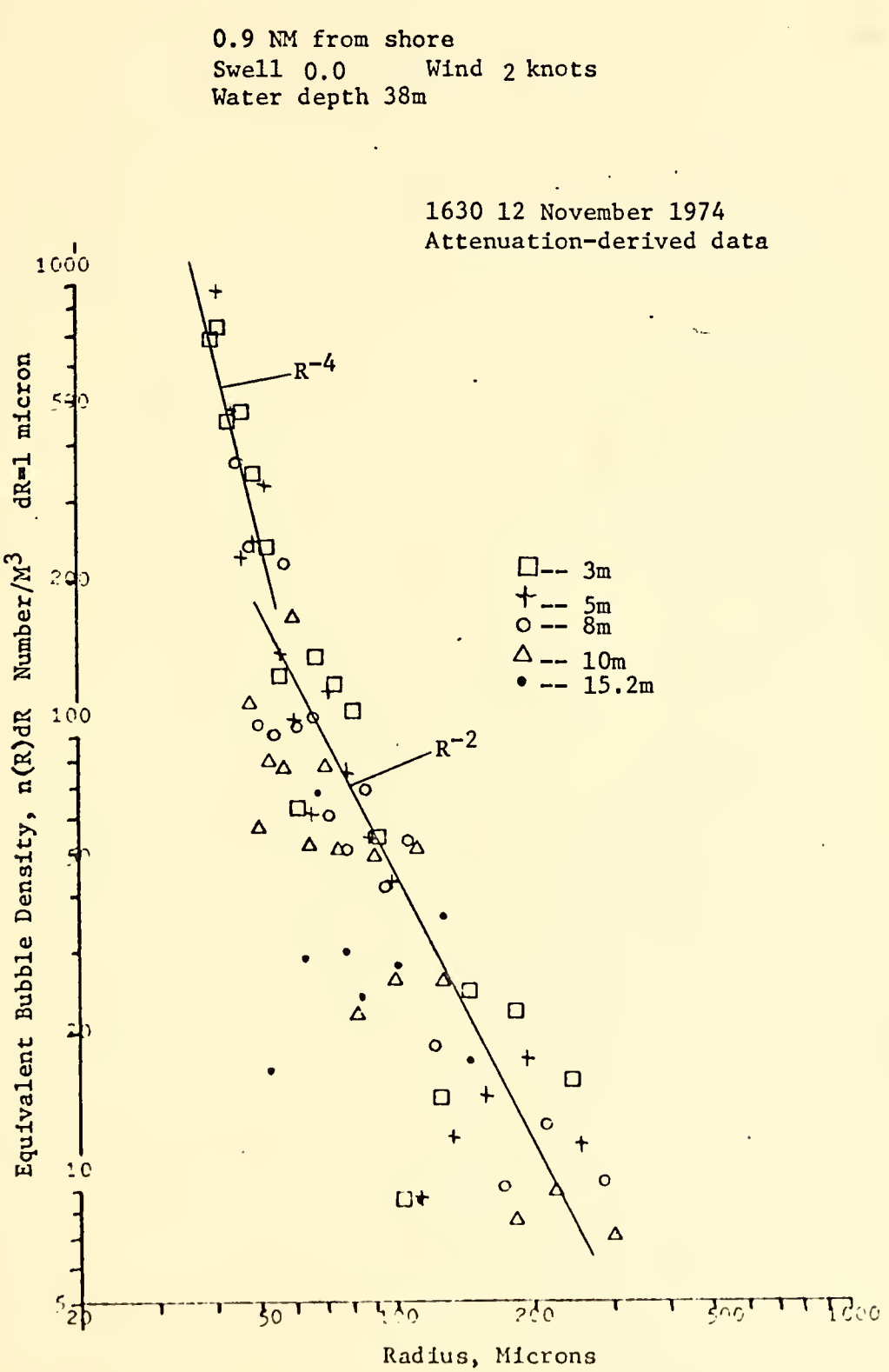

FIG. 12 ATTENUATION-DERIVED BUBBLE POPULATIONS AS A FUNCTION OF BUBBLE RADIUS IN MONTEREY BAY

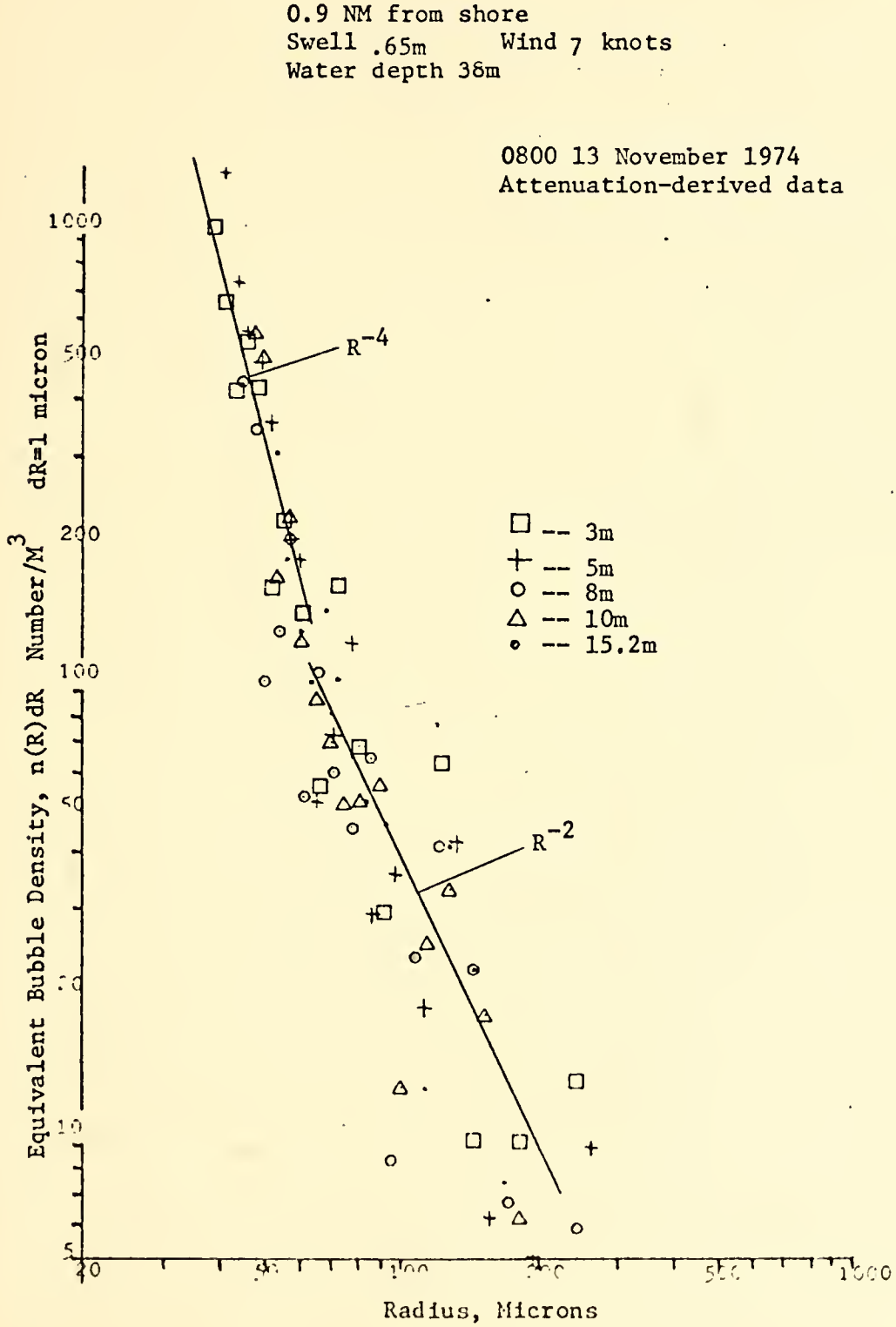

FIG. 13 ATTENUATION-DERIVED BUBBLE POPULATIONS AS A FUNCTION OF BUBBLE RADIUS IN MONTEREY BAY

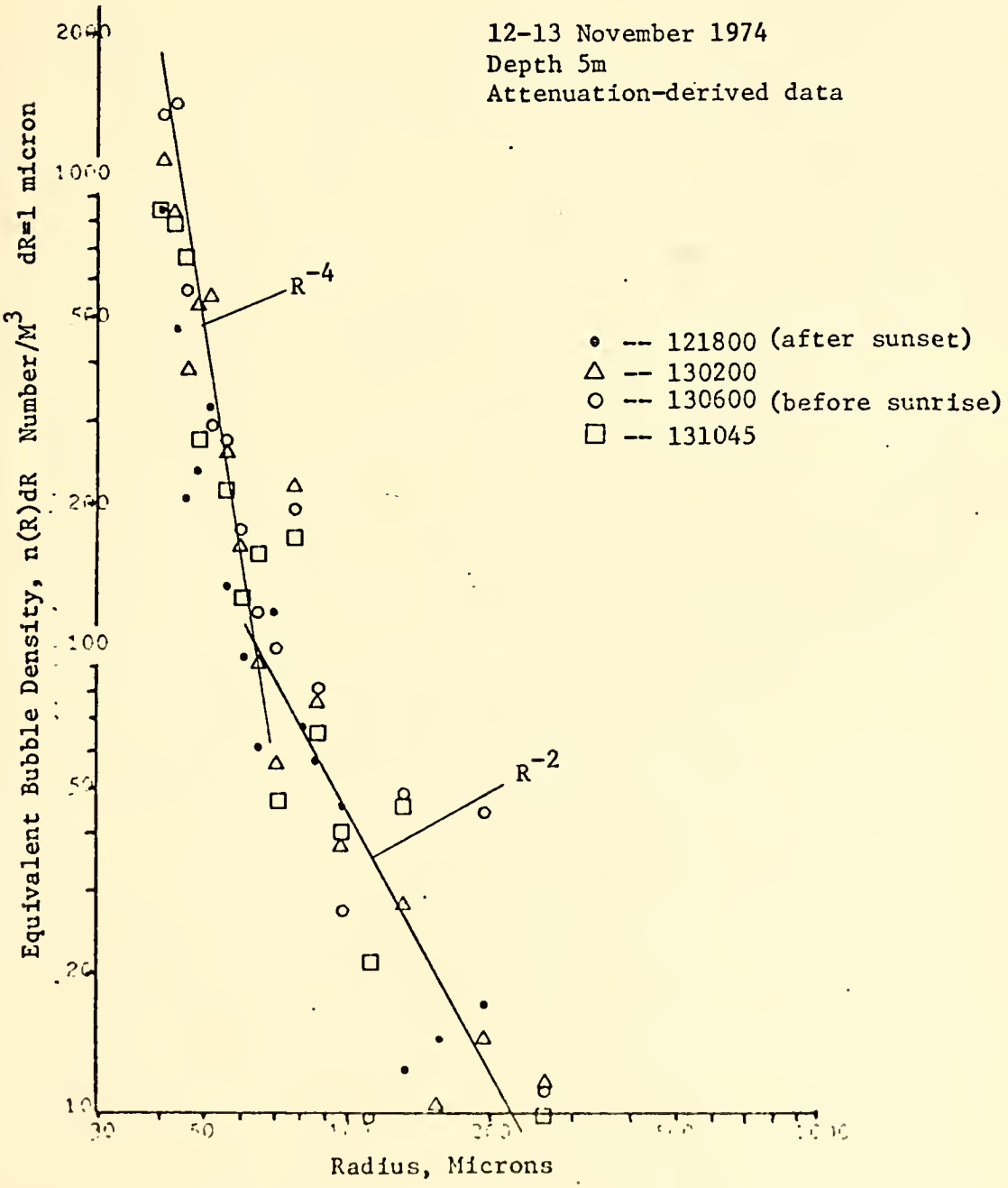

FIG. 14 EXCESS ATTENUATION AND FRACTIONAL BUBBLE-TO-WATER VOLUME AS A FUNCTION OF FREQUENCY IN MONTEREY BAY

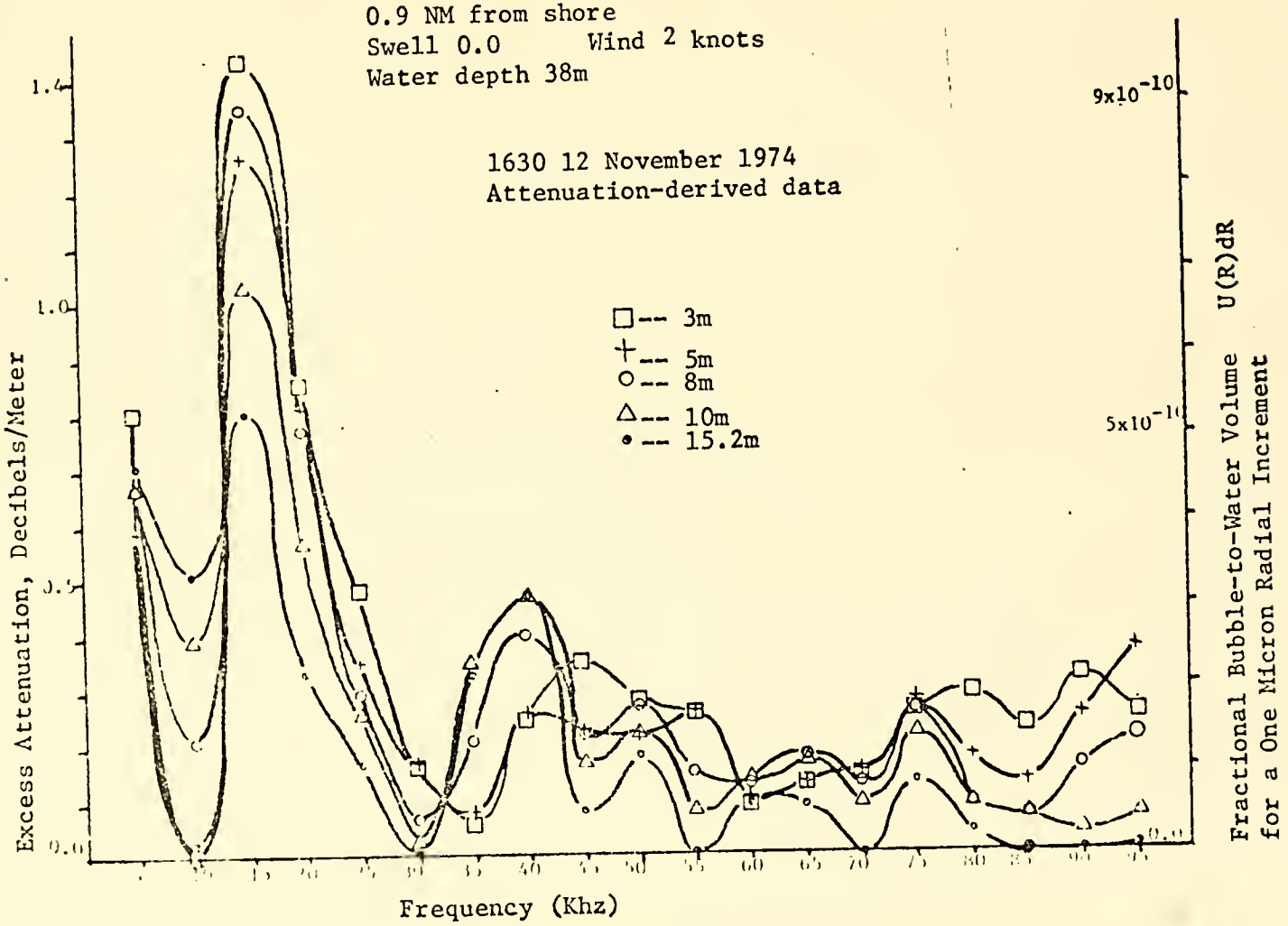

FIG. 15 EXCESS ATTENUATION AND FRACTIONAL BUBBLE-TO-WATER VOLUME AS A FUNCTION OF FREQUENCY IN MONTEREY BAY

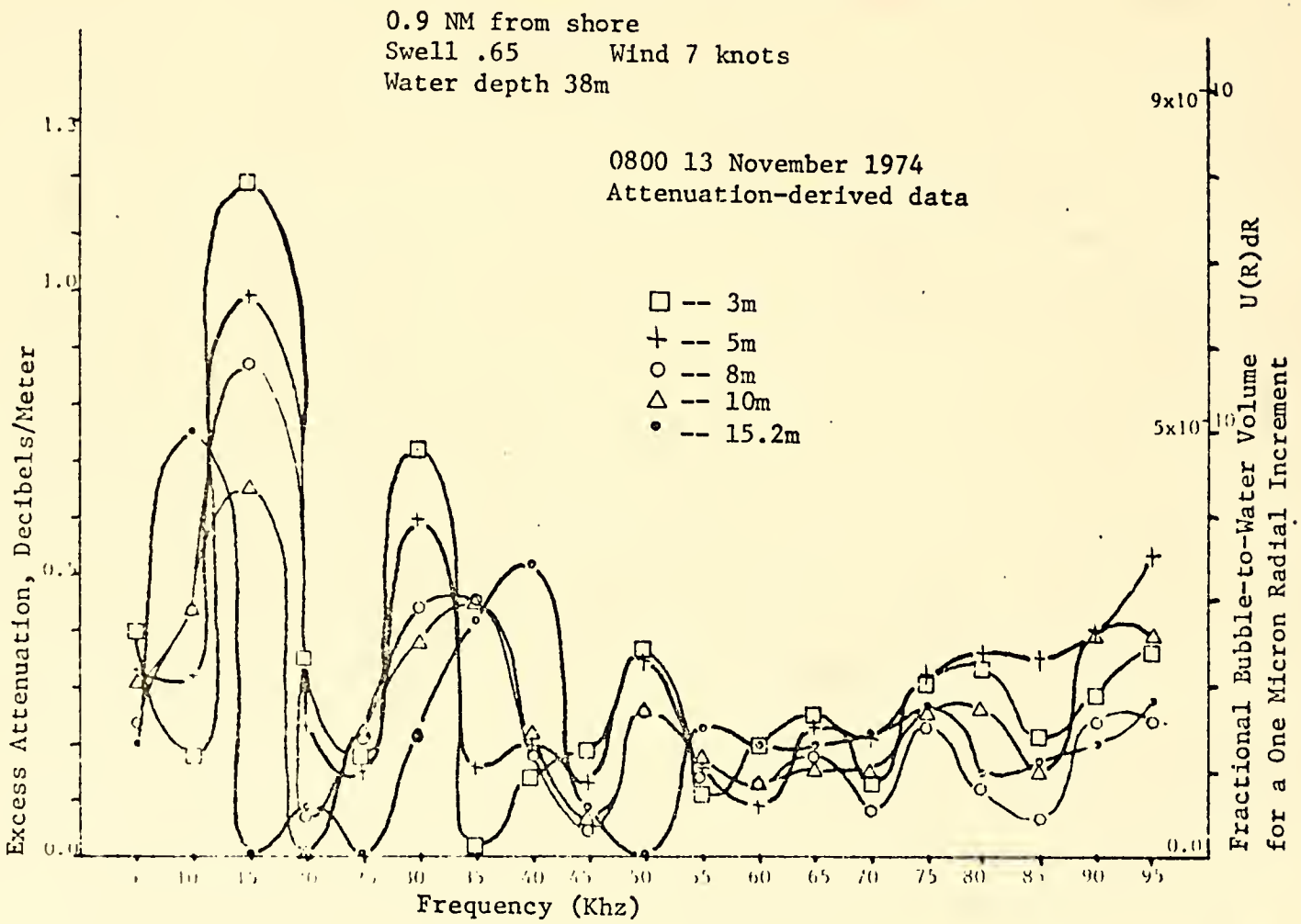

FIG. 16 EXCESS ATTENUATION AND FRACTIONAL BUBBLE-TO-WATER VOLUME AS A FUNCTION OF FREQUENCY AT A CONSTANT DEPTH IN MONTEREY BAY-18 HOUR SURVEY

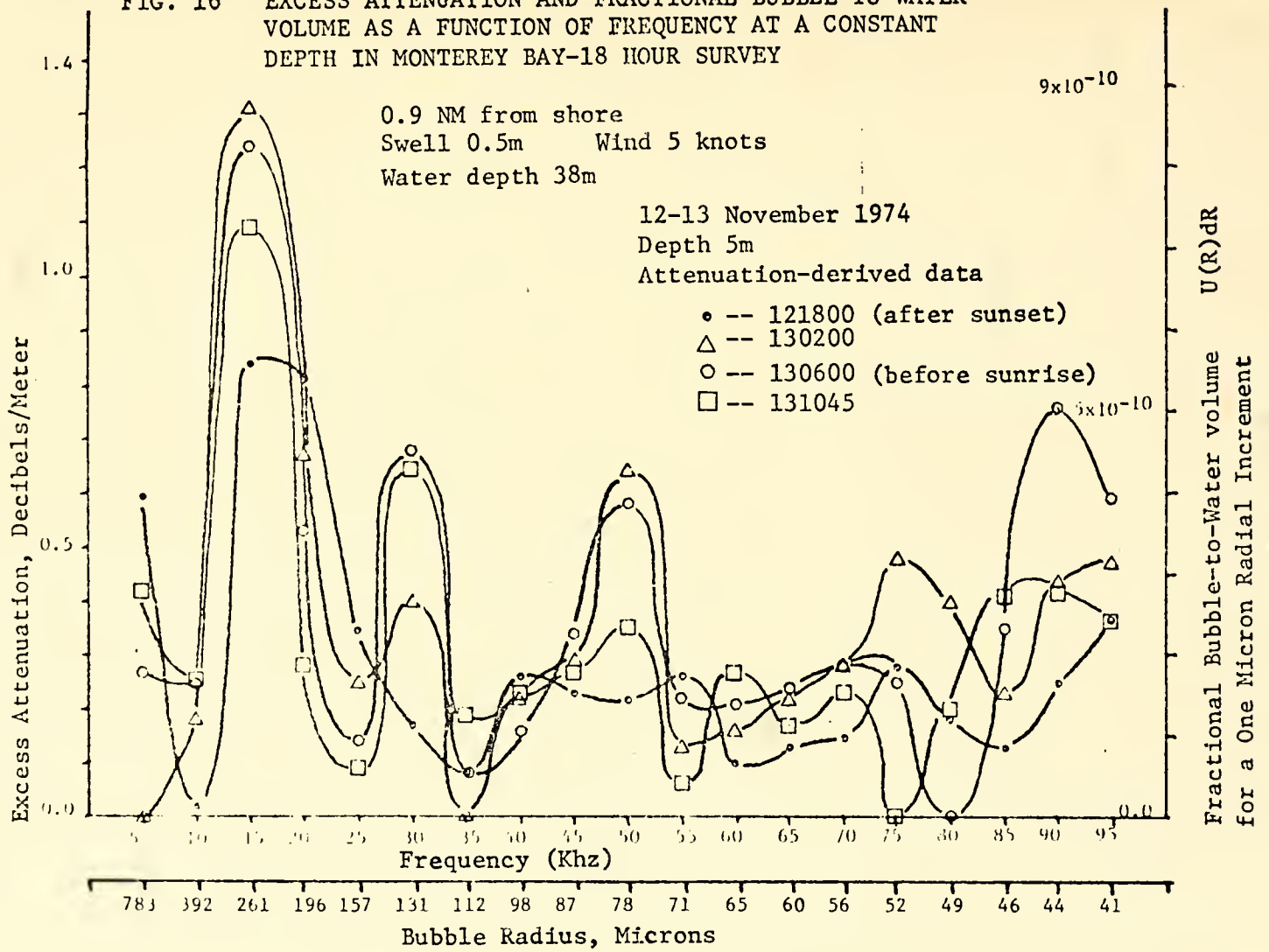

The slight vertical stratification of bubble populations observed during this at-sea experiment is attributed to the 5 knot wind and minimal sea conditions. It is thought that the lack of sea surface agitation significantly reduced the magnitude of expected populations of surface origin in the upper depths.

The presence of bubbles at 15.2 meters is attributed to the relatively shallow water, the in-shore conditions, and the probable biological activity at this location in Monterey Bay.

Finally, although lessened in magnitude due to the use of the nominal reference, Figures 11 and 12 do show trends similar to those found earlier in Mission Bay [Medwin, 1970] as regards rate of increase of bubble populations with decreasing bubble radius. The rate of increase of bubble populations with decreasing bubble radii for bubbles of radii less than 50 microns agreed with the R^{-4} found in the previous work. The number per unit volume of larger bubbles appeared to vary as $R^{-2.4}$ compared with the R^{-2} rate attributable to buoyancy forces found in previous research. Again, there is virtually no bubble range showing Glotov's predicted density proportional to R, due to gas diffusion for R less than 60 microns.

The deviation from trends recorded during previous research was initially thought to be due to test assembly movement in addition to the finite sampling window used in

digital sampling. However, the standard deviation in groups of five runs taken at the same depth over short time periods was consistently 0.1 dB or less.

It is possible to compare the measured speed of sound at low frequencies with the value calculated from bubble populations by using equation (22). The 0200, 13 November 5m depth plot of fractional bubble-to-water volume as a function of bubble radius was used. The area under the curve of U(R) plotted as a function of R was integrated over all bubble radii to arrive at a total fractional air-to-water volume, U.

Equation 21 for ω much less than ω_o gives the asymptotic value of the differential speed

$$c - c_o = \Delta c = -c_o \left[1 - \frac{3U}{2(kR)^2} \right]$$

In the present example,

$$\Delta c = (-1497.18)(3/2)(1642.5\times10^{-10})(1/(1/36\times10^{-2})^2)$$

$$= -1.99 \text{ m/sec.}$$

The bubble-induced change of speed of sound at 10 kHz for the 0200, 13 November run referenced to the 0800 13 November 15.2m run, yields a change in sound speed of -1.2 m/sec. Since different references were used to calculate the attenuation-derived fractional volume and the speed of sound change as obtained from the differential phase, this order-of-magnitude agreement of the two values is reassuring.

3. Sound Speed Dispersion

During each variable-depth series a reference phase angle for each frequency was established using the values from a 50 foot run, previously considered to be bubble-free. A three mHz velocimeter was sampled at each depth to obtain an accurate speed of sound which would account for changes in temperature, salinity, and pressure. By subtracting velocimeter speeds at each depth from those speeds calculated from phase angle computations, changes in the speed of sound which were independent of temperature, salinity, and pressure were obtained. A subsequent plot of the data showed a requirement for an additional correction to compensate for stretching of the monofilament nylon line which was used to pull the two hydrophones together for damping and for constant path length.

The first variable-depth series was taken at 1630 on the afternoon of 12 November 1974, in an area of Monterey Bay sheltered by the Monterey Peninsula from direct ocean swells, Lat. 36°37.7 N, Long. 121°54.1 . Wind speed was two knots, and the swell was negligible. Appendix B itemizes in-situ conditions for each depth. The differential sound speeds, after compensating for velocimeter values and stretch, are shown in Figure 17. Figure 18 shows the standard deviation found at each frequency for the five runs taken at the five meter-depth, which proved to be typical, and for the five runs taken at the eight-meter depth during a later experiment

FIG. 17 SOUND SPEED DISPERSION AS A FUNCTION OF FREQUENCY AT FOUR DEPTHS AT ANCHOR IN MONTEREY BAY

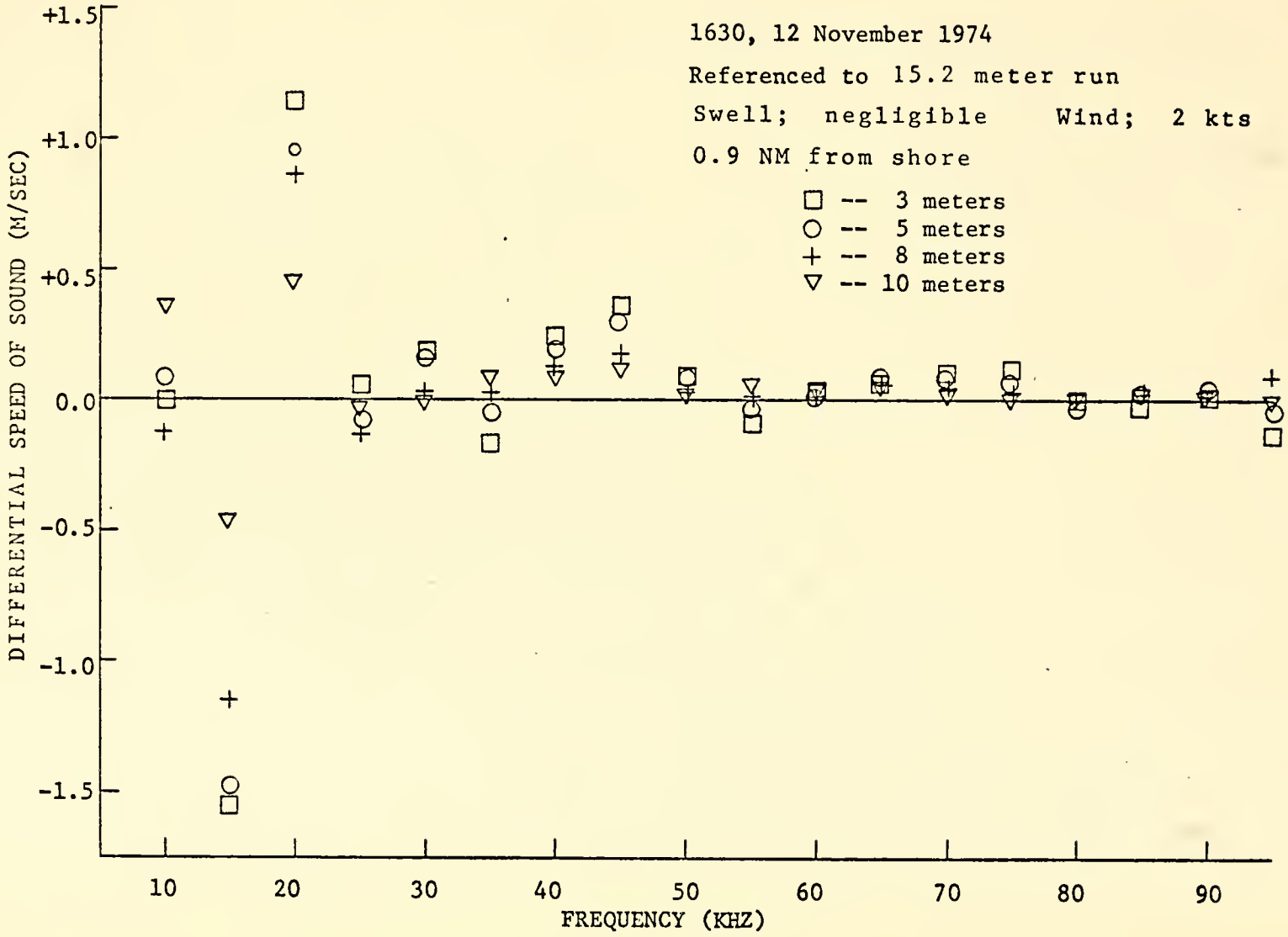

FIG. 18 STANDARD DEVIATION OF SOUND SPEED IN TWO DIFFERENT SEA CONDITIONS

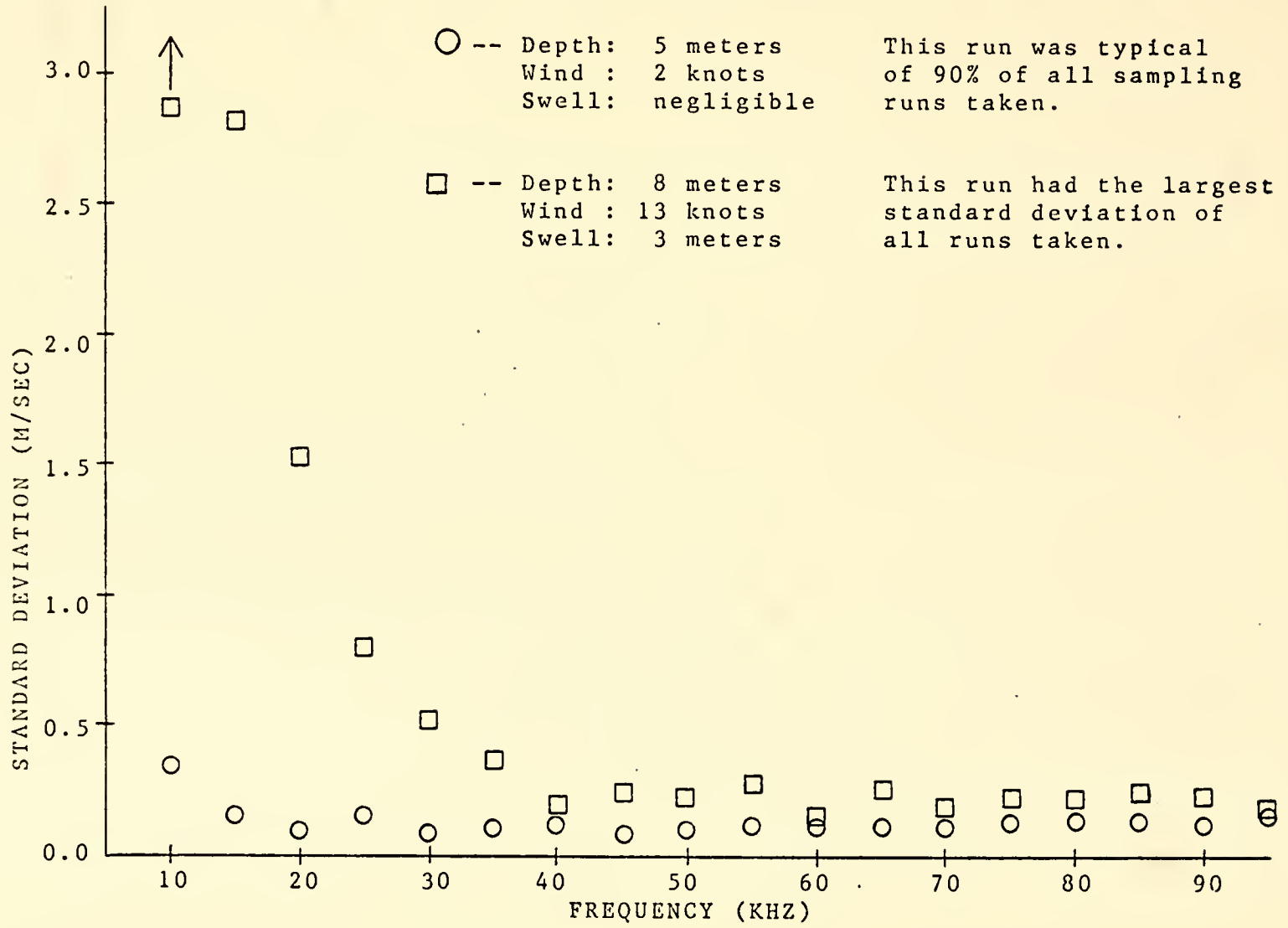

which had the largest standard deviation of all runs taken.

The oscillating differential speeds shown in Figure 17 between 10 kHz and 40 kHz suggest the possibility of a standing waveform being transmitted by the rack at harmonics of the five kHz fundamental frequency. The intensity of this waveform, which alternately increased and decreased the phase angle of succeeding harmonics, displayed a definite depth dependence which overrode meaningful differential speed changes below 45 kHz. Above this frequency the amplitude of this effect decreased sufficiently to permit some observations of a change in sound speed with depth. At 45 kHz the speed increased 0.35 m/sec as the depth changes from 15.2 meters to 3 meters, with consistently increasing values of the sampled speed at intermediate depths. A similar but smaller consistent increase holds between 70 kHz and 75 kHz. At 55 kHz there is a slight but consistent decrease of sound speed between 10 meters and 3 meters. The change of direction of sound speed change with decreasing depth between 55 kHz and 70 kHz, as indicated by a positive slope crossing the axis, suggests an increase in resonant bubble population as the surface was approached with a bubble resonant frequency of approximately 62.5 kHz. A similar presence of resonant bubble populations centered at 17.5 kHz and 27.5 kHz would be suggested except for the overriding harmonic data envelope at those frequencies. A strong resonant bubble

population which increases with decreasing depth can be expected at 45 kHz where the harmonic interference is first overcome by a bubble-dominated response. Plots of excess attenuation versus frequency show resonant bubble populations similar to those predicted by sound speed changes at 15 kHz, 40 kHz, and 65 kHz as predicted, plus peaks at 50 kHz and 75 kHz. The absence of such a population at 30 kHz possibly accounts for the rapid attenuation at that frequency of the overriding harmonic waveform. Discounting the data below 45 kHz, the maximum bubble-induced change in the speed of sound with changing depth at any one frequency is about 0.35 m/sec. Since Appendix B shows the velocimeter sound speed to have changed by 4.69 m/sec during this variable-depth series, it can be seen that sound speed effects caused by variation with depth of temperature, pressure, and salinity exceed those of bubbles under these conditions

A second variable-depth series was taken at the same position commencing at 0800 on the morning of 13 November. Wind speed for this series was seven knots, and the swell was 0.65 meters. Appendix B itemizes in-situ conditions for each depth. The differential sound speeds, after compensating for velocimeter values and stretch, are shown in Figure 19. Again, an overriding oscillating differential speed which changes in intensity with depth is present below 45 kHz. There is again evidence of

FIG. 19 SOUND SPEED DISPERSION AS A FUNCTION OF FREQUENCY AT FOUR DEPTHS AT ANCHOR IN MONTEREY BAY

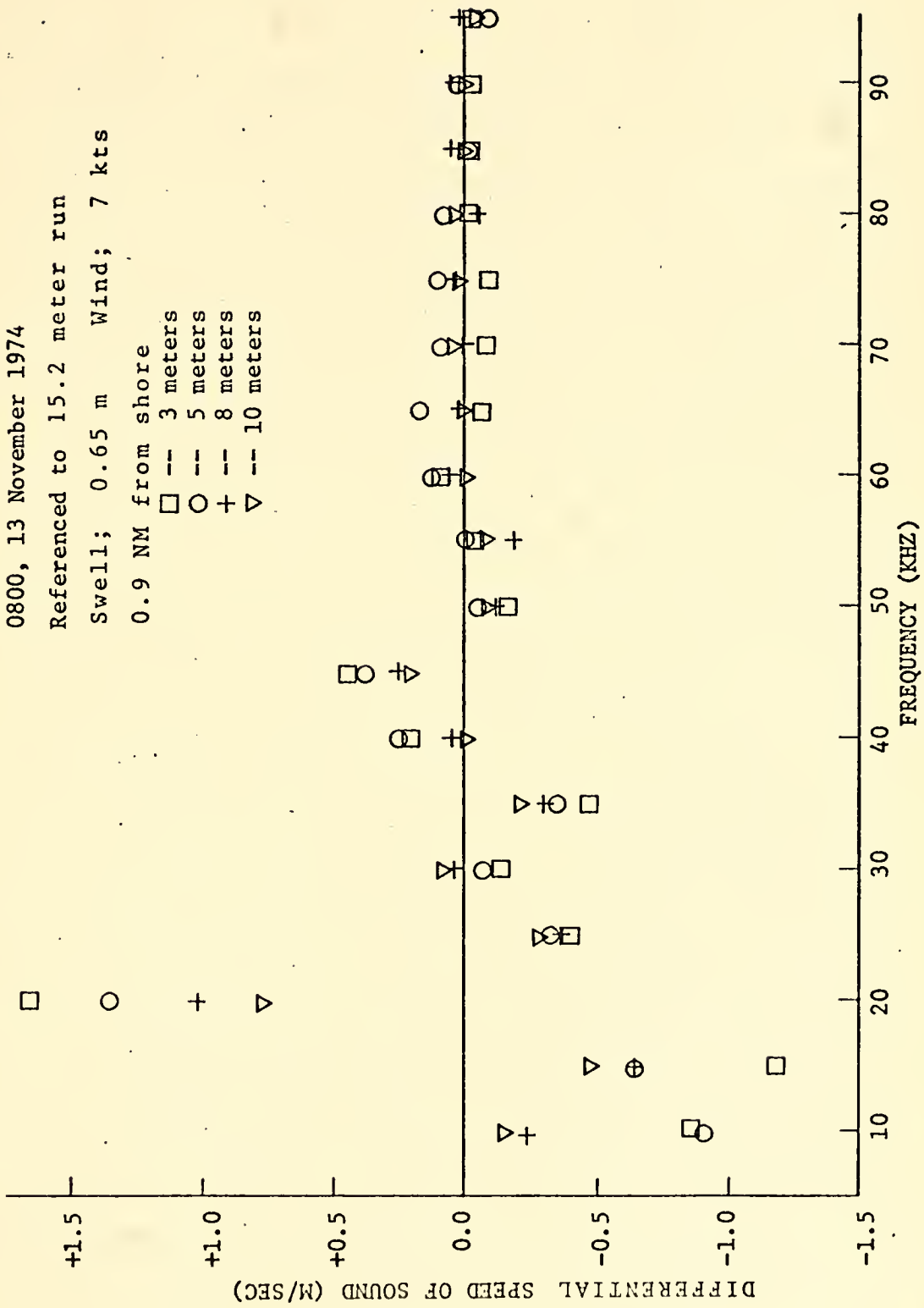

excess resonant bubble populations which increase with a decrease in depth at 45 kHz and 57.5 kHz. A plot of excess attenuation versus frequency shows such a population at 50 kHz and 65 kHz, among others. The maximum bubble-induced differential speed above 40 kHz is 0.5 m/sec. The maximum change in sound speed shown in Appendix B for the velocimeter is 0.45 m/sec during this variable-depth series. This suggests that with sufficient mixing, the bubble effects on the speed of sound are on the same order of magnitude as those of temperature, salinity, and pressure, under these conditions.

Twelve runs were taken at the constant depth of five meters at this same location between the hours of 1600 on 12 November and 1100 on 13 November 1974. The differential sound speeds of three of these runs are shown in comparison to a fourth run at the same depth in Figure 20, to give an indication of the magnitude of bubble induced sound speed changes at one position over a long period of time. These particular times were chosen to show the variations between sunset, nighttime, sunrise, and daytime. By making the reference run one of these runs, any depth dependent rack generated harmonics are eliminated.

From the figure it becomes obvious that although frequency dependent variations are present, they are insignificant in magnitude in this survey. The maximum change in the speed of sound caused by bubbles is 0.8 m/sec, whereas the maximum as indicated by the velocimeter during

FIG. 20 SOUND SPEED DISPERSION AS A FUNCTION OF FREQUENCY AT A CONSTANT DEPTH IN MONTEREY BAY: 18-HOUR SURVEY

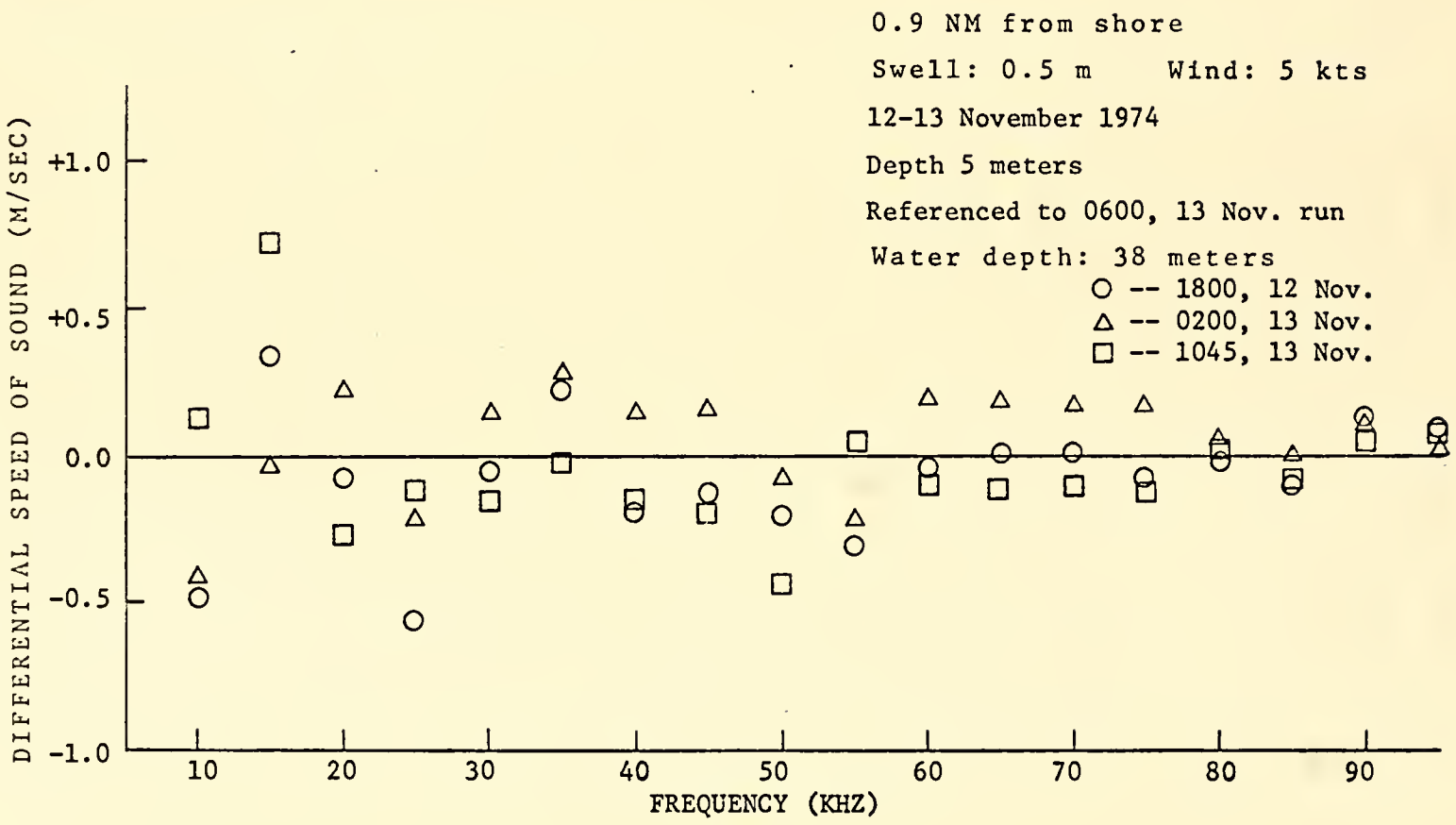

these same four runs is 3.94 m/sec. Since depth, and therefore pressure, was constant during these runs, this suggests that temperature and salinity changes near the surface over a 24-hour period are much more important factors than bubble populations under these conditions.

B. OPEN-OCEAN RESULTS NEAR MONTEREY BAY

A second successful at-sea experiment was conducted on 25 November 1974. This experiment included two variable-depth series in areas unsheltered from ocean swells near Monterey Bay. The first series was taken over Monterey Canyon in 1600 meters of water with the vessel adrift during the experiment. The initial position was Lat. 36 43.5 N, Long. 122 03.1 W, and the position at the end of the series was Lat. 36 43.1 N, Long. 122 02.2 W. During the series the average swell height was three meters, and the average winds were 13 knots. The second series was taken at anchor near the tip of the Monterey Peninsula in 46 meters of water, Lat. 36 38.4 N, Long. 122 57.4 W. During this series, the average swell height was two meters, and the average wind speed was 6 knots. Specific weather and sea conditions are tabulated in Appendix A, and in-situ conditions are tabulated in Appendix B.

1. Procedure

The same equipment set-up was used as described for the 12-13 November experiment, except that the underwater rack Model I was stuffed with steel wool to reduce rack

generated harmonic signals. An initial run at 22.9 meters was used for each variable-depth series to try to find a more nearly bubble-free reference.

2. Amplitude Attenuation

Probing of the 15.2 meter and 22.9 meter depths in search of a bubble-free reference again showed the presence of bubbles at these greatest depths. Even in the deep water run made over the Monterey Canyon, these two depths evidenced bubble populations often in excess of populations found in the near-surface regions. The lowest attenuation was again used as the nominal bubble-free reference as in the previous at-sea run.

Figures 21 and 22 show the number of bubbles per cubic meter in a one micron band as a function of bubble radius for the two vertical series. As in the previous at-sea series conducted 12-13 November, only slight stratification of bubbles with depth was noted. These were unexpected results in view of the deeper water and the increased wind and sea conditions. There was less correlation in slope of the plot with results obtained in previous research in Mission Bay [Medwin, 1970]. Populations of small bubbles below 50 microns varied as $R^{-4.9}$. Larger sized bubbles below 50 microns varied as $R^{-2.5}$. Figures 21 and 22 show marked similarity in slope but exhibit a noticeable difference in point spread. This indicates a more pronounced vertical stratification of bubbles with depth in deeper ocean water further removed from immediate coastal effects.

FIG. 21 ATTENUATION-DERIVED BUBBLE POPULATIONS AS A FUNCTION OF BUBBLE RADIUS OVER MONTEREY CANYON

7.6 NM from shore
Swell 3.0m Wind 13 knots
Water depth 1000m

2000 25 November 1974
Attenuation-derived data

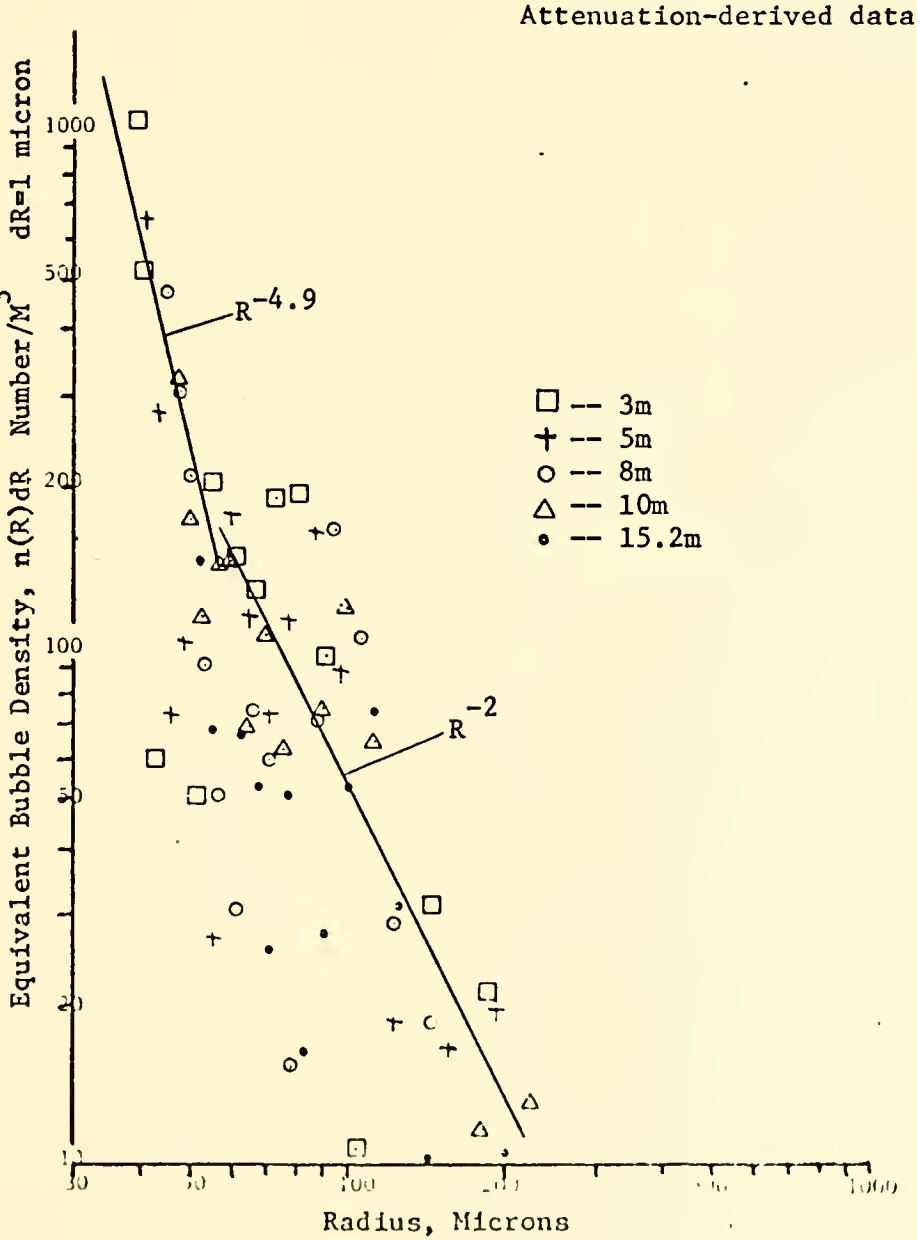

FIG. 22 ATTENUATION-DERIVED BUBBLE POPULATIONS AS A FUNCTION OF BUBBLE RADIUS AT ANCHOR OUTSIDE MONTEREY BAY

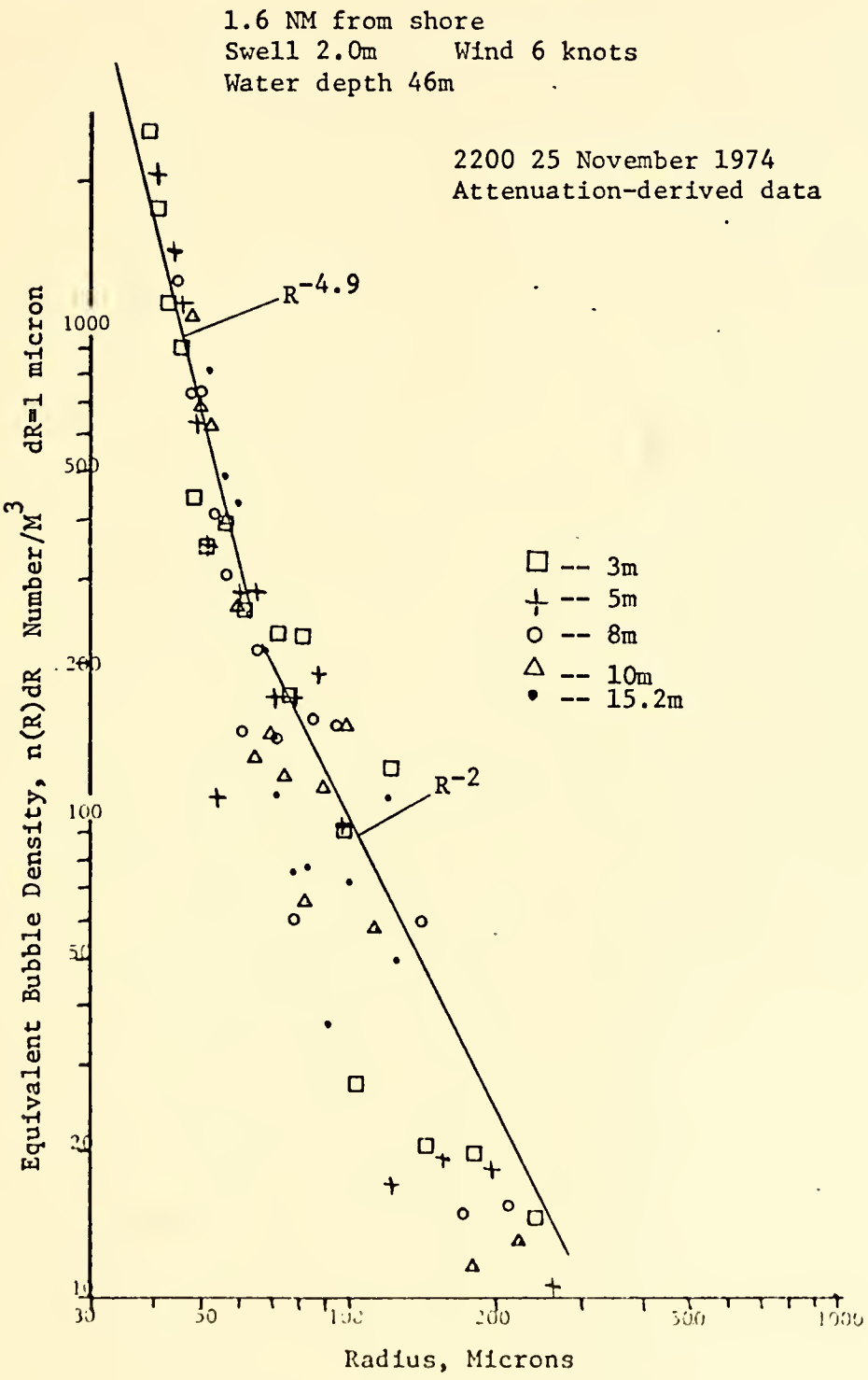

The wind and sea conditions were also more pronounced over the Monterey Canyon which further supports the increased variability in bubble populations.

Figures 23 and 24 show both excess attenuation and fractional volume of air in resonant bubbles as a function of frequency. Strong peaks occur between 15 kHz and 20 kHz and again at 45 kHz. A small maximum is also evidenced at 75 kHz. These attenuation maxima translate to significant bubble populations of radii 200 to 300 microns, 80 to 100 microns, and 50 to 60 microns, depending upon depth. These bubble maxima are supported by the phase analysis calculations used to compute sound speed dispersion.

3. Sound Speed Dispersion

The differential sound speeds obtained during the variable depth series taken over Monterey Canyon are shown in Figure 25. The positive slopes crossing the axis in the vicinity of 40 kHz and 75 kHz indicate increasing bubble populations with decreasing depth. The eight-meter run shows a large resonant bubble population at 18 kHz, not seen at the other depths. A plot of excess attenuation versus frequency confirms that such populations exist at 20 kHz, 45 kHz, and to a very small extent at 75 kHz. The greatest change in the differential sound speed at any one frequency was 3.01 m/sec at 10 kHz, which was obtained during the eight-meter run. This run consistently had a much larger standard deviation than normal (see Figure 18),

FIG. 23 EXCESS ATTENUATION AND FRACTIONAL BUBBLE-TO-WATER VOLUME AS A FUNCTION OF FREQUENCY OVER MONTEREY CANYON

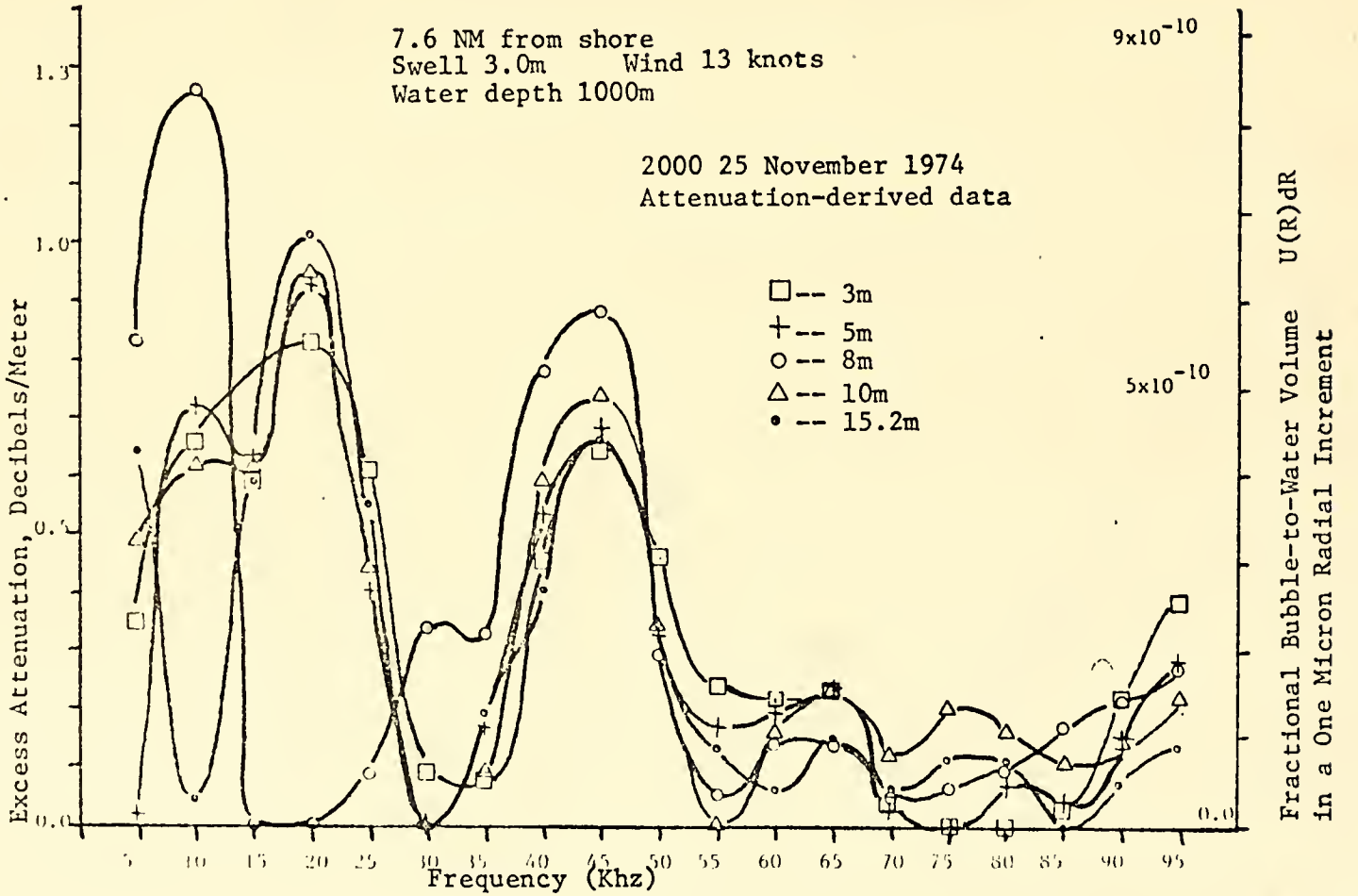

FIG. 24 EXCESS ATTENUATION AND FRACTIONAL BUBBLE-TO-WATER VOLUME AS A FUNCTION OF FREQUENCY AT ANCHOR OUTSIDE MONTEREY BAY

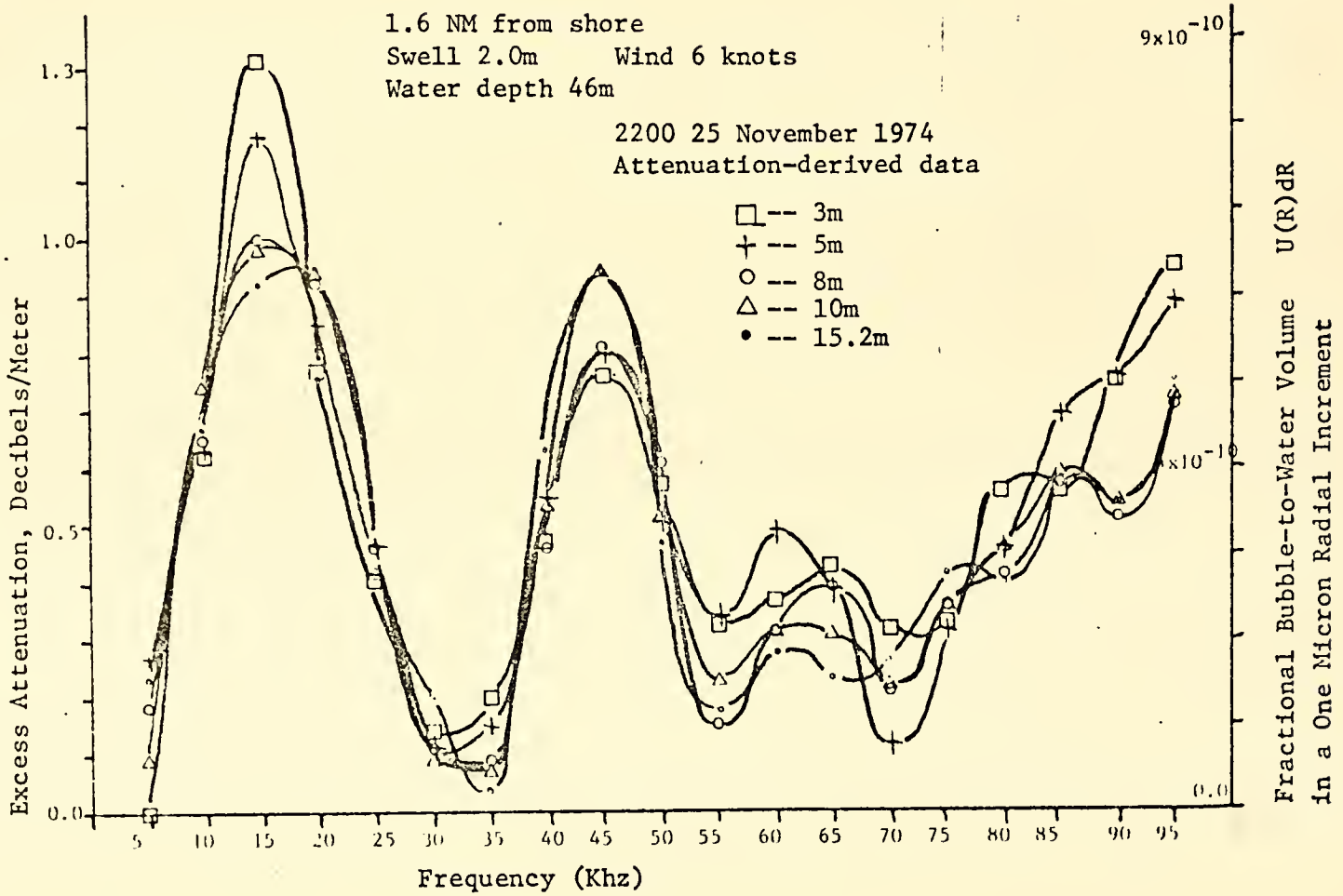

FIG. 25 SOUND SPEED DISPERSION AS A FUNCTION OF FREQUENCY AT FOUR DEPTHS DRIFTING OVER MONTEREY CANYON

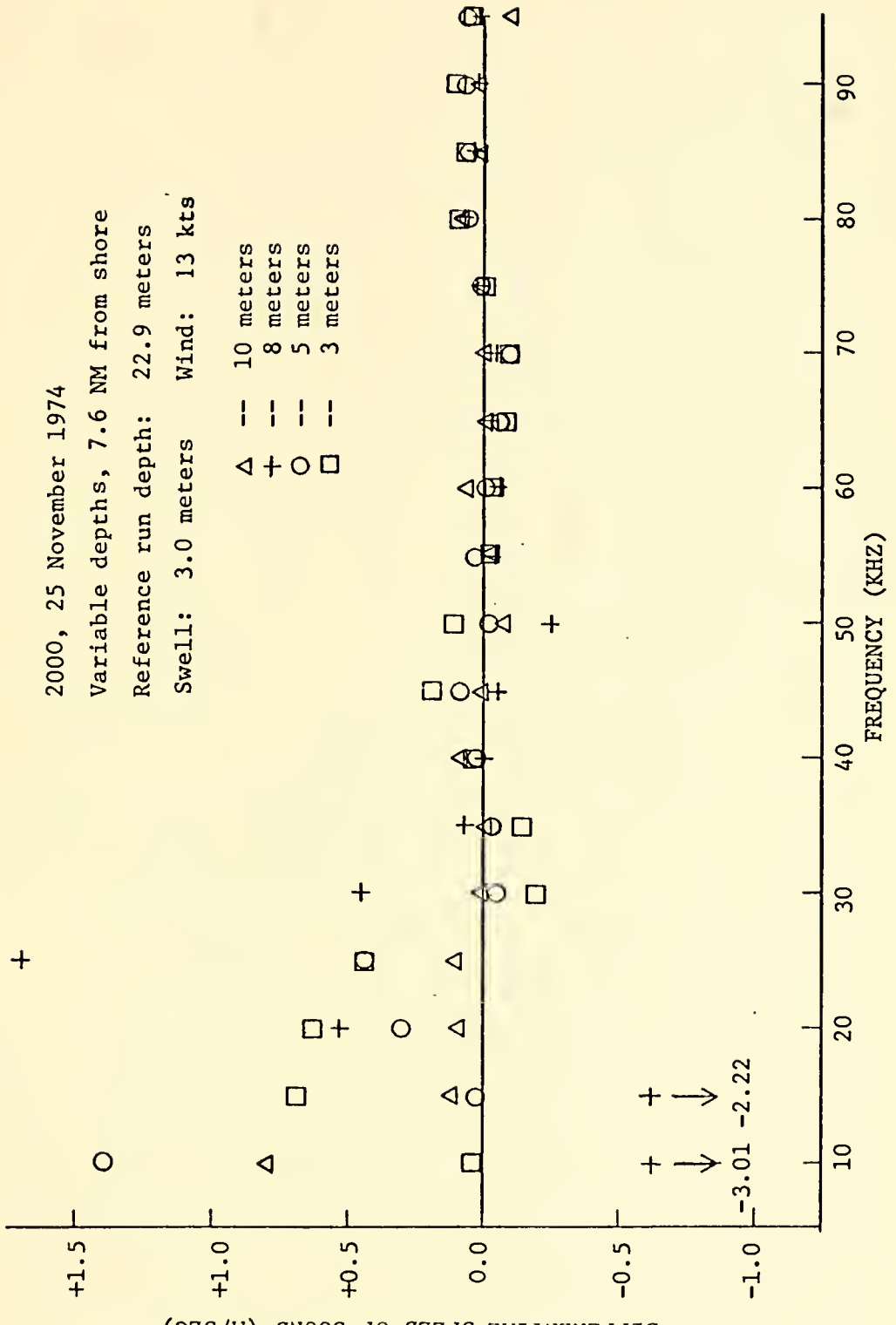

reaching a maximum of 3.66 m/sec at 10 kHz. If this run is discounted because of its excessive variation, the maximum differential sound speed is 1.4 m/sec. Appendix B lists the velocimeter-obtained variation of sound speed with depth as 0.3 m/sec, suggesting that bubble-induced sound speed variations with frequency under these mixed water conditions are more significant than those caused by temperature, pressure, and salinity changes.

The differential sound speeds obtained while at anchor off the tip of Monterey Peninsula are shown in Figure 26. Positive slopes cross the axis at 17.5 kHz, 40 kHz, and 75 kHz. Excess attenuation plots confirm large resonant bubble populations at 15 kHz and 45 kHz, but show consistently increasing bubble populations with increasing frequency above 70 kHz, with no unusually large populations around 75 kHz. The maximum differential sound speed which can be attributed to bubbles is 0.8 m/sec.

FIG. 26 SOUND SPEED DISPERSION AS A FUNCTION OF FREQUENCY AT FOUR DEPTHS AT ANCHOR OUTSIDE MONTEREY BAY

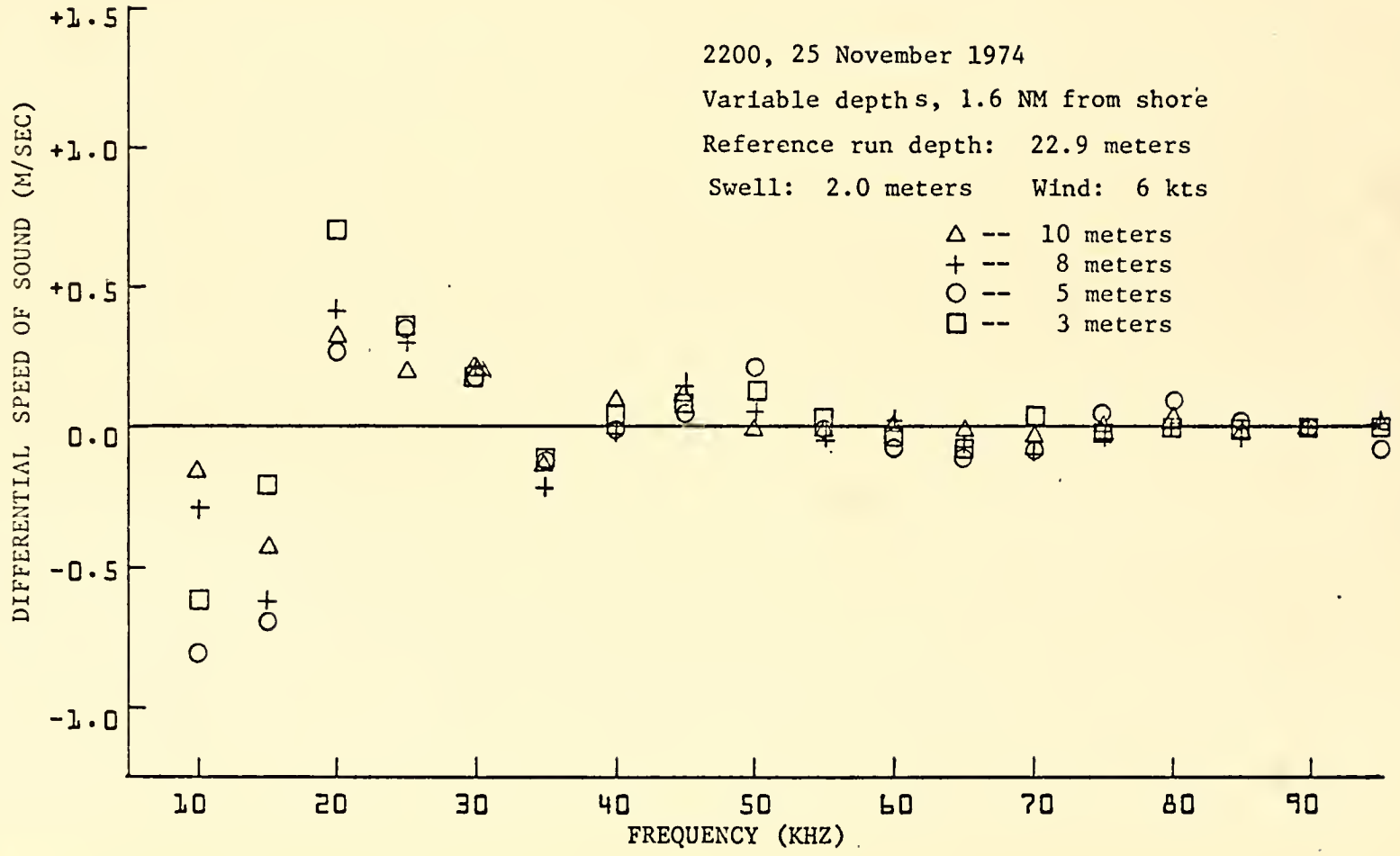

VII. SUMMARY AND CONCLUSIONS

A portable transducer-hydrophone system with a fixed path length between two hydrophones of 0.95 meters was used to study the in-situ speed of sound and sound pressure amplitude attenuation as a function of frequency over the range of 5 kHz to 95 kHz. These experiments permitted the calculation of microbubble density variations with depth and also at a constant depth over an 18-hour sampling period at three different locations in and near Monterey Bay. This study was of interest in determining the error caused by omitting frequency dependence in traditional ray tracing methods of determining sound paths.

The experiments were conducted in water depths of 38 meters, 46 meters, and 1000 meters, in sea states one and two. Phase and amplitude measurements were taken at depths of 22.9 meters, 15.2 meters, 10 meters, 8 meters, 5 meters, and 3 meters. An 18-hour survey was also taken at a constant depth of 5 meters in 38 meters of water.

Analysis of amplitude attenuation in the upper depths of the ocean shows the definite presence and effect of resonant microbubble populations. However, the magnitude of the bubble population and its distribution throughout the medium is a function of many parameters. At all locations probed during this research work, a complicated dependence of bubble densities on depth was found. In some

cases there was greater attenuation at 15.2 meters than at 3 meters. Apparent peaks in bubble population, as evidenced by a large excess attenuation, were noted but showed no obvious correlation with wind or sea conditions. The lack of significant increase in bubble populations with increase in wind and sea conditions may be attributable to the principal attenuation sources being biological rather than physical. It is expected that under conditions of increased agitation, the near-surface bubble populations would be significantly higher.

Changes in the speed of sound which could be attributed to bubbles were obtained by subtracting the speed of sound as indicated by a 3 MHz velocimeter from that obtained from in-situ phase angle measurements. These changes were plotted as a differential speed of sound for each variable-depth series, referenced to the speed at the deepest position sampled. They were also plotted for four of the constant-depth runs of the 18-hour survey referenced to one of those four runs.

Analysis of these data indicated that the relative importance to the speed of sound in water of resonant bubbles compared to the traditional parameters of temperature, depth, and salinity is very dependent on the degree of mixing of the water. There was little indication of any relationship between bubble-induced sound speed changes and wave height when all frequencies were considered. A larger differential sound speed occurred in the heaviest

sea state at the lower frequencies, with a maximum value of 3.01 m/sec at 10 kHz. During the same series the maximum sound speed change caused by other parameters was only 0.3 m/sec.

The changes of sound speed with depth at various frequencies were of sufficient magnitude to suggest the need for a thorough in-situ study of the sound speed dispersion with depth in all possible sea conditions at the frequencies of any proposed or existing surface ship sonar. Such a study would determine if the need exists for modification of predicted performance characteristics in surface duct propagation.

APPENDIX A

SEA SURFACE AND ATMOSPHERIC CONDITIONS

November 1974 (Date/Time)	Wind Direction (° True)	Wind Velocity (Knots)	Barometric Pressure (Inches Hg)	Predominant Swell Dir/Ht/Period (° True/Meters/Sec)			Cloud Cover (%)	Comments
12/1700	305	2	30.10	None			50	Sunset
12/1800	170	3	30.10	300	.25	10	80	Thousands of squid visible
13/0200	085	4	30.08	320	1.00	7	40	Dozens of squid visible
13/0600	105	3	30.09	330	.35	8	25	Two 70-ft. fishing boats within 100 meters
13/0900	035	7	30.11	310	.65	11	70	Two 70-ft. fishing boats within 100 meters
13/1100	250	2	30.11	350	.65	10	50	
25/1900	310	13	30.16	310	3.00	12	00	Drifting over Monterey Canyon
25/2200	310	6	30.16	310	2.00	11	00	At anchor

APPENDIX B

IN-SITU VELOCIMETER SPEED, WATER TEMPERATURE, AND FLOW RATES

Series Type	November 1974 (Date/Time)	Velocimeter Values: Sound Speed (M/Sec)	Velocimeter Values: Water Temperature (° C)	Flow Meter Values: Vertical Flow (Ft/Sec)	Flow Meter Values: Sound-Path Flow (Ft/Sec)	Depth (Meters)	Comments
Variable Depth Series (1630)	12/1629	1493.23	16.35	± .1	.1	15.2	
	12/1651	1494.42	16.19	± .1	.2	10	Sunset at 1700
	12/1717	1494.98	16.44	± .1	.2	8	
	12/1800	1496.08	16.41	± .1	.1	5	Thousands of squid visible
	12/1823	1497.92	16.38	± .1	.1 ± .1	3	Thousands of squid visible
Variable Depth Series (0800)	13/0800	1496.28	16.42	± .2	.1	15.2	Two fishing boats w/i 100 m.
	13/0847	1496.23	16.42	± .2	.1	10	Two fishing boats w/i 100 m.
	13/0906	1496.38	16.29	± .2	-.1	8	No boats in vicinity
	13/0927	1496.28	16.44	± .1	.1	5	
	13/0950	1496.73	16.44	± .1	.1	3	
Constant Depth Survey	13/0200	1497.18	16.50	± .2	.1	5	See also 12/1800 above
	13/0600	1496.93	16.45	± .2	.1	5	Sunrise 0645
	13/1045	1496.38	16.41	± .4	.2 ± .2	5	

Variable Depth Series (2000)	25/1852	1495.18	16.75	± 1.0	1.2 ± .4	22.9	Drifting over Monterey Canyon
	25/1910	1495.38	16.73	± 1.0	1.0 ± .4	15.2	
	25/1929	1495.48	16.69	± 1.5	1.0 ± .3	10	
	25/1944	1495.43	16.74	± 1.3	1.2 ± .4	8	
	25/1958	1495.43	16.71	± 1.4	.8 ± .2	5	
	25/2012	1495.43	16.71	± 1.4	.4 ± .2	3	
Variable Depth Series (2200)	25/2129	1495.08	16.55	± 1.5	.4	22.9	At anchor outside Monterey Bay
	25/2146	1495.58	16.55	± 1.5	.4	15.2	
	25/2200	1495.58	16.53	± 1.2	.6 ± .2	10	
	25/2211	1495.58	16.53	± 1.0	.4 ± .2	8	
	25/2224	1495.58	16.52	± 1.1	.4 ± .2	5	
	25/2236	1495.68	16.52	± 1.6	.3 ± .3	3	

COMPUTER OUTPUT

A. TRUNCATED SAMPLING PROGRAM OUTPUT

```
INPUT VALUE OF N ? (00=END)

10
NO COMPLEX PTS = 1024

INPUT SAMPLE FREQ ?
320000.00
WHICH PSDS ?
16

INPUT LIST DESIRED
0
PSD PRINTOUT ?
1
RECORD OUTPUT ?
0
DTG ? (MMDDHHMM)
11251116
CONTINUE ?
1
CONTINUE ?
1
```

CHANNEL NO. 1

PSD	FREQ	ANGLE
5340721.0	0.000	0.000
15795.3	2500.000	249.212
23666960.0	5000.000	66.134
2507.4	7500.000	22.017
72514992.0	10000.000	324.187
3921.0	12500.000	187.480
219777424.0	15000.000	245.620
1628.2	17500.000	41.477
210713616.0	20000.000	214.703
2013.8	22500.000	270.819
486584320.0	25000.000	110.488
700.3	27500.000	195.660
674972672.0	30000.000	33.018
330.8	32500.000	44.748
767184384.0	35000.000	321.074
5289.4	37500.000	15.938
801828608.0	40000.000	249.923
5569.3	42500.000	311.331
912102912.0	45000.000	185.057
8900.6	47500.000	235.892
1061476608.0	50000.000	113.195

CHANNEL NO. 2

PSD	FREQ	ANGLE
82337472.0	0.000	180.000
47583.3	2500.000	230.611
6556624.0	5000.000	4.232
1048.7	7500.000	136.263
55263504.0	10000.000	215.251
1060.5	12500.000	81.730
69656592.0	15000.000	69.685
765.8	17500.000	115.068
134958672.0	20000.000	286.427
1910.6	22500.000	337.068
169702384.0	25000.000	154.724
277.0	27500.000	76.382
281499648.0	30000.000	19.399
244.4	32500.000	267.951
286739968.0	35000.000	248.680
1310.3	37500.000	337.081
394425856.0	40000.000	115.001
2201.2	42500.000	155.977
461564672.0	45000.000	339.063
277.8	47500.000	8.576
457626624.0	50000.000	202.138

FREQ	1 OLDG(PSD1/PSD2)	ANGLE1-ANGLE2
0.000	11.87998	-180.000
2500.000	4.78928	18.601
5000.000	-5.57462	61.902
7500.000	-3.78566	-114.246
10000.000	-1.17989	108.937
12500.000	-5.67874	105.751
15000.000	-4.99021	175.935
17500.000	-3.27612	-73.592
20000.000	-1.93492	-71.724
22500.000	-0.22831	-66.250
25000.000	-4.57470	-44.237
27500.000	-4.02882	119.279
30000.000	-3.79809	13.619
32500.000	-1.31372	-223.204
35000.000	-4.27411	72.394
37500.000	-6.06043	-321.143
40000.000	-3.08116	134.921
42500.000	-4.03139	155.354
45000.000	-2.95811	-154.006
47500.000	-15.05754	227.316
50000.000	-3.65399	-88.943

B. TRUNCATED AVERAGING PROGRAM OUTPUT

```
END OF PROGRAM / (0=NO,1=YES)
0
NO. OF FREQUENCIES ? (12)
33
DTG ? (MMDDHHMM)  (0000=LAST)
11251130
DTG ? (MMDDHHMM)  (0000=LAST)
11251133
DTG ? (MMDDHHMM)  (0000=LAST)
11251135
DTG ? (MMDDHHMM)  (0000=LAST)
11251137
DTG ? (MMDDHHMM)  (0000=LAST)
11251141
DTG ? (MMDDHHMM)  (0000=LAST)
0000
NO. OF DTG'S = 5
MAKE SURE DATA TAPE IS READY
CONTINUE ?
```

FREQ	LOG(PSD) MEAN	LOG(PSD) STD	ANGLE MEAN	ANGLE STD
0.0	12.11756	0.40824	180.00000	0.00000
5000.0	-5.48554	0.28456	65.43140	1.17339
10000.0	-2.93204	0.07189	114.37544	0.61215
15000.0	-5.07862	0.0883	179.05240	0.55400
20000.0	-2.15473	0.11825	290.79907	0.32653
25000.0	-4.98481	0.12138	319.27783	0.45279
30000.0	-4.18389	0.03636	18.11159	0.68177
35000.0	-4.81204	0.02665	75.50655	0.40488
40000.0	-3.54478	0.03717	137.50362	0.53174
45000.0	-3.67428	0.04034	210.35587	0.86080
50000.0	-4.75935	0.07145	271.59082	0.70619

COMPUTER PROGRAMS

A. SAMPLING PROGRAM

```
      SUBROUTINE FOUR1(DATA,N,ISIGN)
C     THE COOLEY-TUKEY FAST FOURIER TRANSFORM IN USASI BASIC FORTRAN.
C     NOTE--IT SHOULD NOT BE NECESSARY TO CHANGE ANY STATEMENTS IN THIS
C     PROGRAM SO LONG AS THE FORTRAN COMPILER USED STORE REAL AND
C     IMAGINARY PARTS ADJACENTLY IN STORAGE.
C     TRANSFORM(K) = SUM(DATA(J)*EXP(ISIGN*2*PI*SQRT(-1)*(J-1)*(K-1)
C     /N)), SUMMED OVER ALL J AND K FROM 1 TO N.  DATA IS A ONE-
C     DIMENSIONAL COMPLEX ARRAY (I.E., THE REAL AND IMAGINARY PARTS
C     ARE ADJACENT IN STORAGE, SUCH AS FORTRAN IV PLACES THEM) WHOSE
C     LENGTH N=2**K, K.GE.0 (IF NECESSARY, APPEND ZEROES TO THE DATA).
C     ISIGN IS +1 DR -1.  IF A -1 TRANSFORM IS FOLLOWED BY A +1 ONE (OR
C     VICE VERSA) THE ORIGINAL DATA REAPPEAR, MULTIPLIED BY N.  TRANSFORM
C     VALUES ARE RETURNED IN ARRAY DATA, REPLACING THE INPUT.  THE TIME
C     IS PROPORTIONAL TO N*LOG2(N), RATHER THAN THE NAIVE N**2.
C     ACCURACY IS ALSO GREATLY IMPROVED.  THE RMS RELATIVE ERROR BEING
C     BOUNDED BY 6*SQRT(2)*LOG2(N)*2**(-B), WHERE B IS THE NUMBER OF
C     BITS IN THE FLOATING POINT FRACTION.  WRITTEN BY NORMAN BRENNER OF
C     MIT LINCOLN LABORATORY.  JULY 1967.  THIS IS THE SHORTEST VERSION
C     OF THE FFT KNOWN TO THE AUTHOR.  FASTER PROGRAMS FOUR2 AND
C     FOURT EXIST THAT OPERATE ON ARBITRARILY SIZED MULTIDIMENSIONAL
C     ARRAYS.  SEE--IEEE AUDIO TRANSACTIONS (JUNE 1967), SPECIAL ISSUE
C     ON FFT.
```

```
      DIMENSION DATA(1)
      IPO=2
      IP3=IP0*N
      I3REV=1
      DO 50 I3=1,IP3,IP0
      IF(I3-I3REV) 10,20,20
10    TEMPR=DATA(I3)
      TEMPI=DATA(I3+1)
      DATA(I3)=DATA(I3REV)
      DATA(I3+1)=DATA(I3REV+1)

      DATA(I3REV)=TEMPR
      DATA(I3REV+1)=TEMPI
20    IP1=IP3/2
30    IF(I3REV-IP1) 50,50,40
40    I3REV=I3REV-IP1
      IP1=IP1/2
      IF(IP1-IP0) 50,30,30
50    I3REV=I3REV+IP1
      IP1=IP0
60    IF(IP1-IP3) 70,100,100
70    IP2=IP1*2
      THETA=6.283185307/FLOAT(ISIGN*IP2/IP0)
      SINTH=SIN(THETA/2.)
      WSTPR=-2.*SINTH*SINTH
      WSTPI=SIN(THETA)
      WR=1.
      WI=0.
      DO 90 I1=1,IP1,IP0
      DO 80 I3=I1,IP3,IP2
      I2A=I3
      I2B=I2A+IP1
      TEMPR=WR*DATA(I2B)-WI*DATA(I2B+1)
      TEMPI=WR*DATA(I2B+1)+WI*DATA(I2B)
      DATA(I2B)=DATA(I2A)-TEMPR
      DATA(I2B+1)=DATA(I2A+1)-TEMPI
```

```
      DATA(I2A)=DATA(I2A)+TEMPR
 80   DATA(I2A+1)=DATA(I2A+1)+TEMPI
      TEMPR=WR
      WR=WR*WSTPR-WI*WSTPI+WR
 90   WI=WI*WSTPR+TEMPR*WSTPI+WI
      IP1=IP2
      GO TO 60
100   RETURN
      END
```

```
      PING1D     24 OCTOBER 1974     OCH

      THIS PROGRAM TAKES DATA FROM TWO ADC CHANNELS,PERFORMS
      AN FFT ON IT,CALCULATES PSD AND ANGLES,PRINTS ONLY
      SPECIFIED PEAKS,THEN CALCULATES 10LDG10(PSD1/PSD2)
      AND THE DIFFERENCE BETWEEN THE ANGLES FOR EACH CHANNEL

      THIS PROGRAM WILL RECORD TO TAPE, IF REQUESTED,
      THE FREQUENCY, 10LDG(PSD2/PSD1), AND THE ANGLE
      DIFFERENCES FOR THE DESIRED FREQUENCIES.  IT ALSO
      REQUESTS AND PUTS ON TAPE AN EIGHT-DIGIT IDENTIFICATION
      NUMBER.

      THIS PROGRAM HAS THE ABILITY TO USE UP TO 1024
      DATA POINTS PER CHANNEL

      IARY IS THE ANALOG ARRAY (INTEGER)
      ARY IS THE REAL DATA ARRAY
      N IS THE POWER OF 2 EQUAL TO THE ARRAY SIZE
      1 = YES, 0 = NO

      INTEGER*2 IARY
      DIMENSION IARY(2,1030),ARY(2,1024)
      DIMENSION OUT (2,515)
      EQUIVALENCE (OUT(1,1),IARY(1,1))
      IEND1 = 2

      CLEAR IARY

800   DO 10 I=1,1024
      IARY(1,I) = 9
      IARY(2,I) = 9
10    CONTINUE
```

```
          REQUEST INPUT PARAMETERS

16         WRITE(3,300)
 300      FORMAT (/28HINPUT VALUE OF N ? (00=END) )
          READ (5,301) N
 301      FORMAT (I2)
          IF (N.EQ.0) GO TO 860
          IF (N.GT.10)GO TO 16
          NV=2**N
          INV=(NV/2)+2
          WRITE (3,310) NV
 310      FORMAT(17HNO COMPLEX PTS = ,I4)
          WRITE(3,315)
315       FORMAT(/19HINPUT SAMPLE FREQ ?)
           READ(5,316) SF
 316      FORMAT (F8.4)
         WRITE(3,850)
 850     FORMAT(13HWHICH PSDS ?)
         READ(5,301)IPSD
         WRITE(3,302)
302       FORMAT(/18HINPUT LIST DESIRED)
         READ(5,350)IL
 350     FORMAT (I1)
         WRITE (3,462)
```

```
462     FORMAT (15HPSD PRINTOUT ?)
        READ (5,350) IP
         WRITE(3,303)
        READ(5,350)IT
303     FORMAT (16HRECORD OUTPUT ?)
        WRITE (3,900)
900     FORMAT (17HDTG ? (MMDDHHMM) )
        READ (5,901) ID1,ID2
901     FORMAT (2I4)
        IF (IT.EQ.0) GO TO 950
        WRITE (2,901) ID1,ID2

        COMPUTE RESOLUTION AND TOTAL BANDWIDTH

950     FPSD = FLOAT(IPSD)
        RES = FPSD/(FLOAT(NV)*(1.0/SF))
         TB=1.0/(2.0*(1.0/SF))
        WRITE (3,870)
870     FORMAT (11HCONTINUE ?)
        READ (5,350) ICO
        IF (ICO.EQ.0) GO TO 800

        INPUT DATA ON CHANNEL B/C ADC
        192 = HEX C0

        NVV = NV+2
        IOC = 192
        CALL ADCDAC(IOC,IARY,NVV)

         ADC DATA NOW IN

        WRITE (3,870)
        READ (5,350) ICO
        IF (ICO.EQ.0) GO TO 800
        INX = 2*NV
```

```
      TRANSFER TO COMPLEX ARRAY

 8    DO 15 KCHAN=1,2
      WRITE (3,320) KCHAN
320    FORMAT(//12HCHANNEL NO. ,I1//)
      IF (KCHAN.EQ.2) GO TO 400
      DO 1 I=1,NV
      II = I+2
      ARY(1,I) = FLOAT(IARY(KCHAN,II))
 1    ARY(2,I)=0.0
      GO TO 490
 400  DO 410 I=1,NV
      IARY(2,I) = IARY(2,I+2)
 410  CONTINUE
      KK = (NV+4)/2
      OUT(1,KK) = ARY(1,KK)
      OUT(2,KK) = ARY(2,KK)
      OUT(1,KK-1) = ARY(1,KK-1)
      OUT(2,KK-1) = ARY(2,KK-1)
      K = NV
      DO 420 I=1,NV,2
      KK = K/2
      TEMP1 = FLOAT(IARY(2,K))
      TEMP2 = FLOAT(IARY(2,K-1)
```

```
        OUT(1,KK) = ARY(1,KK)
        OUT(2,KK) = ARY(2,KK)
        ARY(1,K) = TEMP1
        ARY(2,K) = 0.0
        ARY(1,K-1) = TEMP2
        ARY(2,K-1) = 0.0
        K = K-2
420     CONTINUE

490     IF (IL-1) 7,6,7

6       DO 3 I=1,NV,8
        II = 1+7
        WRITE (3,602) (ARY(1,M),M=I,II)
602     FORMAT (8F7.0)
3         CONTINUE

7       IX = -1
         CALL FOUR1(ARY,NV,IX)
        IF (IP.EQ.0) GO TO 611
        WRITE (3,610)
610     FORMAT (16X,3HPSD,13X,4HFREQ,6X,5HANGLE/)
611     RS = 0.0

        OUTPUT LIST = 1/2 NO. COMPLEX POINTS +2

        DO 2 I=1,INV,IPSD
        IF (ARY(1,I).NE.0.0)GO TO 500
        IF (ARY(2,I))501,502,503
501     ANGLE = 270.0
        GO TO 530
502     ANGLE=0.0
        GO TO 530
```

```
503     ANGLE=90.0
        GO TO 530
500     ANGLE=ATAN(ARY(2,I)/ARY(1,I))
        ANGLE = ANGLE*57.29577951
        IF (ARY(1,I).GE.0.0) GO TO 505
        ANGLE = ANGLE+180.0
        GO TO 530
505     IF (ARY(2,I).GE.0.0) GO TO 530
        ANGLE = ANGLE+360.0
530     PSD = ARY(1,I)*ARY(1,I)+ARY(2,I)*ARY(2,I)
        IF (IP.EQ.0) GO TO 612
        WRITE (3,600) PSD,RS,ANGLE
612     ARY(1,I) = PSD
        ARY(2,I) = ANGLE
600     FORMAT (3X,F16.1,3X,F14.3,3X,F8.3)
         IF(RS.LT.TB) GOTO 20
        RS=0.0
        GOTO 2
20       RS=RS+RES
2       CONTINUE

15      CONTINUE
```

```
      RS = 0.0
      WRITE (3,460)
460   FORMAT (/13X,4HFREQ,3X,16H10LOG(PSD1/PSD2),3X,13HANGLE1-ANGLE2/)

      DO 430 I=1,INV,IPSD
      IF (ARY(1,I).NE.0.0) GO TO 450
      PSD = 9999.0
      GO TO 451
450   PSD = 10.0*ALOG10(ARY(1,I)/OUT(1,I))
451   ANGLE = OUT(2,I)-ARY(2,I)
      IF (IT.EQ.1) GO TO 442
      WRITE (3,461) RS,PSD,ANGLE
      GO TO 441
442   WRITE (2,461) RS,PSD,ANGLE
441   IF (RS.LT.TB) GO TO 440
      RS = 0.0
      GO TO 430
440   RS = RS+RES
430   CONTINUE
461   FORMAT (3X,F14.3,3X,F16.5,3X,F13.3)

      IF (IT.EQ.0) GO TO 800
      CALL EOF(IEND1)
       GO TO 800
860   IF (IT.EQ.0) GO TO 861
     CALL EOF(IEND1)
861   STOP
      END
```

B. AVERAGING PROGRAM

```
MSDPA1      29 OCTOBER 1974      CCH

THIS PROGRAM WILL PROCESS THE TAPES WRITTEN BY
PING1D BY COMPUTING THE MEAN AND STANDARD DEVIATION
OF SPECIFIED GROUPS OF DATA

A MAXIMUM OF SEVEN (7) DATE/TIME GROUPS MAY BE
ENTERED AT ONE TIME

A MAXIMUM OF 35 FREQUENCIES ARE ALLOWED

INTEGER*2 DTG
DIMENSION FREQ(7,35),PSD(7,35),ANGLE(7,35)
DIMENSION DTG(7,3)
```

```
      ************************
      REQUEST INPUT PARAMETERS
      ************************

100   WRITE (3,900)
900   FORMAT  (30HEND OF PROGRAM ? (0=NO,1=YES))
      READ (5,901) IEND
901   FORMAT (I1)
      IF (IEND.EQ.1) GO TO 230

105   WRITE (3,920)
920   FORMAT (26HNO. OF FREQUENCIES ? (I2))
      READ (5,921) NF
921   FORMAT (I2)
      IF (NF.GT.35) GO TO 105
      J = 1
110   WRITE (3,902)
902   FORMAT (29HDTG ? (MMDDHHMM) (0000=LAST))
      READ (5,903) DTG(J,1),DTG(J,2)
903   FORMAT (2I4)
      IF (DTG(J,1).EQ.0) GO TO 120
      J = J+1
      IF (J.GE.8) GO TO 115
      GO TO 110
115   WRITE (3,912)
912   FORMAT (22HMAX NO. DTG'S ENTERED)
120   J = J-1
      WRITE (3,904) J
904   FORMAT (14HNO. OF DTG'S = ,I2)
      WRITE (3,906)
906   FORMAT (28HMAKE SURE DATA TAPE IS READY)
      WRITE (3,905)
905   FORMAT (11HCONTINUE ?)
      READ (5,901) ICO
      IF (ICO.EQ.0) GO TO 100
```

```
      ********************************
      FIND AND READ IN SPECIFIED DTG'S
      ********************************

      DO 150 I=1,J
125   READ (2,903) ID1,ID2
      IF (ID1.NE.DTG(I,1)) GO TO 140
      IF (ID2.NE.DTG(I,2)) GO TO 140

      DO 130 I2=1,NF
      READ (2,907) FREQ(I,I2),PSD(I,I2),ANGLE(I.I2)
907   FORMAT (3X,F14.3,3X,F16.5,3X,F13.3)
      IF (I.EQ.1) GO TO 130
      IF (FREQ(I,I2).NE.FREQ(1,I2) GO TO 160
130   CONTINUE
      GO TO 150

140   CALL SEOF
      GO TO 125
150   CONTINUE
      GO TO 170
160   WRITE (3,909)
909   FORMAT (29HFREQUENCIES DO NOT CORRESPOND)
      GO TO 100
```

```
      ************************************
      CALCULATE MEAN AND STANDARD DEVIATION
      ************************************

170   WRITE (3,908)
908   FORMAT (/5X,4HFREQ,2X,13HLOG(PSD) MEAN,3X,12HLOG(PSD) STD,
     15X,1OHANGLE MEAN,6X,9HANGLE STD)

      DIV = FLOAT(J)
      DO 210 I2=1,NF
      SUMA = 0.0
      SUMP = 0.0
      DO 190 I=1,J
      SUMP = SUMP+PSD(I,I2)
      IF (ANGLE(I,I2).LT.0.0) ANGLE(I,I2)=ANGLE(I,I2)+360.0
      SUMA = SUMA+ANGLE(I,I2)
190   CONTINUE
      AVGP = SUMP/DIV
      AVGA = SUMA/DIV
      SUMA = 0.0
      SUMP = 0.0
      DO 200 I=1,J
      DIFFA = ANGLE(I,I2)-AVGA
      DIFFP = PSD(I,I2)-AVGP
      SUMA = SUMA+(DIFFA*DIFFA)
      SUMP = SUMP+(DIFFP*DIFFP)
200   CONTINUE
```

```
      STDA = SQRT(SUMA/DIV)
      STDP = SQRT(SUMP/DIV)
      WRITE (3,910) FREQ(1,Iw),AVGP,STDP,AVGA,STDA
910   FORMAT (1X,F8.1,4(1X,F14.5))
210   CONTINUE

220   WRITE (3,911)
911   FORMAT (//)
      GO TO 100


      **************
      END OF PROGRAM
      **************
```

BIBLIOGRAPHY

1. Alexander, C. H., Sound Phase and Amplitude Fluctuations in an Anisotropic Ocean, M.S. Thesis, U.S. Naval Postgraduate School, 1972.

2. Blanchard, D.C. and Woodcock, A. H., "Bubble Formation and Modification in the Sea and its Meteorological Significance," Tellus, v. 9, p. 145-158, 1957.

3. Buxcey, S., McNeil, J. E., and Mark, R. H., Jr., Acoustic Detection of Microbubbles and Particulate Matter near the Sea Surface, M.S. Thesis, U.S. Naval Postgraduate School, 1965.

4. Devin, Charles, Jr., "Survey of Thermal, Radiation and Viscous Damping of Pulsating Air Bubbles in Water," Journal of the Acoustic Society of America, v. 31, p. 1654-1667, 1959.

5. Fitzgerald, J. R., Statistical Study of Sound Speed in the Inhomogeneous Upper Ocean, M.S. Thesis, U.S. Naval Postgraduate School, 1973.

6. Glotov, V. P., et al., "Investigation of the Scattering of Sound by Bubbles Generated by an Artificial Wind in Sea Water and the Statistical Distribution of Bubble Sizes," Soviet Physics-Acoustics, v. 7, p. 341-345, 1962.

7. Medwin, Herman, "In Situ Acoustic Measurements of Bubble Populations in Coastal Ocean Waters," Journal of Geophysical Research, v. 75-3, p. 599-611, 20 January 1970.

8. Medwin, H., Rautmann, J., and Fitzgerald, J. R., "Acoustic Mini-Probing for Ocean Microstructure and Bubbles," Journal of Geophysical Research, scheduled for publication 20 Jan. 1975.

9. Medwin, H., Notes on Underwater Acoustics: Attenuation due to Multiple Bubbles, dated 1964.

10. Rautmann, J., Sound Dispersion and Phase Fluctuations in the Upper Ocean, M.S. Thesis, U.S. Naval Postgraduate School, 1972.

11. Smith, W. J., Jr., Amplitude Modulation of an Acoustic Wave Propagating near the Sea Surface, M.S. Thesis, U.S. Naval Postgraduate School, 1972.

INITIAL DISTRIBUTION LIST

		No. Copies
1.	Defense Documentation Center Cameron Station Alexandria, Virginia 22314	2
2.	Library, Code 0212 Naval Postgraduate School Monterey, California 93940	2
3.	Department Chairman, Code 61 Department of Physics and Chemistry Naval Postgraduate School Monterey, California 93940	2
4.	Professor H. Medwin, Code 61 Md Department of Physics and Chemistry Naval Postgraduate School Monterey, California 93940	10
5.	LT Dennis Leeth Zveare 714 Tantallon Drive Tantallon-on-Potomac, Maryland 20022	1
6.	LT Thomas Bartlett Huffman 208 Hickory Drive Shelbyville, Tennessee 37160	1
7.	Office of Naval Research Code 480 800 Quincy Arlington, Virginia 22217	1
8.	Department Chairman, Code 58 Department of Oceanography Naval Postgraduate School Monterey, California 93940	1
9.	Mr. William Smith Department of Physics and Chemistry Naval Postgraduate School Monterey, California 93940	1
10.	Dr. J. Harris Pinkerton Computer Consultants, Inc. 65 West Street Road Warminster, Pennsylvania 18974	1

11. Mr. T. H. Lee — 1
Pinkerton Computer Consultants, Inc.
65 West Street Road
Warminster, Pennsylvania 18974

12. Mr. J. J. Kacergis — 1
Special Projects Group
Naval Air Development Center
Warminster, Pennsylvania 18974

13. Assoc. Professor E. D. Traganza, Code 58 Tg — 1
Department of Oceanography
Naval Postgraduate School
Monterey, California 93940

14. LCDR C. R. Dunlap, Code 58 Du — 1
Department of Oceanography
Naval Postgraduate School 93940

15. Professor Eugene C. Haderlie — 1
Department of Oceanography
Naval Postgraduate School
Monterey, California 93940

16. Naval Sea Systems Command — 1
Department of the Navy
PMS 06H1-4 ATTN: Mr. A. Franceschetti
Washington, D. C. 20362

17 Dr. Morris Schulkin — 1
Associate Director
Naval Oceanographic Office
Washington, D.C. 20390

18. Dr. Joseph Dickie — 1
Naval Ship Research and Development Center
Annapolis, Maryland 21402

19. Dr. J. B. Hersey — 1
Office of Naval Research (Code 102-05)
Department of the Navy
Washington, D.C. 20360

20. Dr. D. Weston — 1
Group D
Admiralty Research Laboratory
Teodington, Middlesex
London, England

21. Dr. H. Bezdek — 1
Office of Naval Research (Code 486)
800 Quincy
Arlington, Virginia 22217

22. Dr. Bachmann — 1
c/o SACLANT ASW Research Centre
APO New York, New York 09019

23. Dr. L. P. Atkinson — 1
Research Associate
Skidway Institute of Oceanography
University System of Georgia
55 West Bluff Road
Savannah, Georgia 31406

24. Dr. J. Berkson and Dr. O. I. Diachok — 1
Code 8050
Naval Research Laboratory
Washington, D. C. 20375